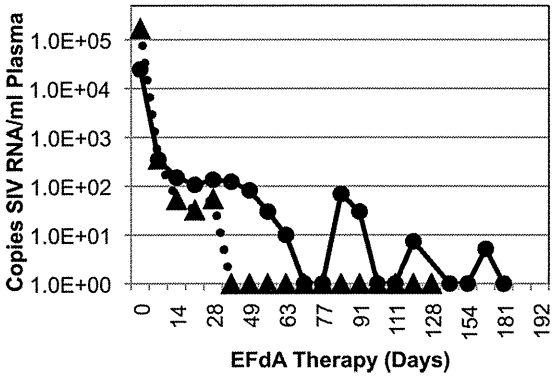

FIG 3 *In vivo* response of SIV/DeltaB670 to EFdA treatment. Virus loads during EFdA therapy, excerpted from Fig. 2, are shown for better resolution. Therapy consisted of twice-daily subcutaneous injections of 0.4 mg/kg. Values from monkey R395 are indicated by triangles connected by the dashed line. The circles connected by the solid line reflect the values from monkey R393.

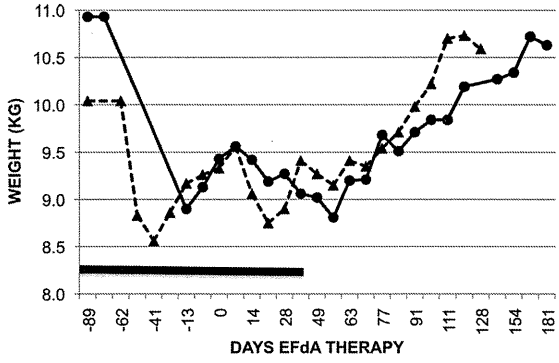

FIG 4 Effect of EFdA therapy on diarrhea and weight loss. Monkeys were observed daily in their cages for normal stool and weighed at weekly or biweekly intervals. Stool consistency was graded +1 (fully formed), +2 (loose), +3 (watery with no solids), or +4 (bloody). The black line depicts the interval of +3 grade stool. Weight is measured in kilograms. The triangles connected by the dashed line present weights of monkey R395. Circles connected by the solid line represent weights of monkey R393.

R393 (6 months total) and then discontinued. After discontinuation of the drug, a rebound in virus was observed in R393 that continued until his sacrifice 2 months later.

Viral resistance. Although there was no obvious sign of emerging resistance to EFdA during treatment, the sporadic blips of viremia observed in monkey R393 suggested that, despite treatment, virus replication had continued in some unknown reservoir. This suspicion was further substantiated by the rebound of virus after EFdA was discontinued. We therefore obtained a partial sequence of the viral RT (nucleotides 3353 to 3682) from plasma virions at two time points during the study, 2 weeks prior to initiation of EFdA treatment, and during the postdrug rebound. We had previously determined that the rebounded virus after TFV plus lopinavir-ritonavir therapy did not contain the K65R mutation (24 and unpublished data). As expected, of 12 clones obtained 2 weeks before EFdA treatment, all contained wild-type virus. Sixty days after the discontinuation of EFdA therapy, however, the rebound virus contained 2 significant changes, conversion of the methionine at position 184 to either valine or isoleucine (M184V and M184I, respectively; 6 of 12 clones). Although these mutations are well known for conferring resistance to other NRTIs (23, 25), they did not result in a significant change in virus burden during EFdA therapy. Whether treatment with a higher dose of EFdA or a more prolonged therapy would have had a greater impact on infection and disease will require further study with a larger cohort of animals.

Effect of EFdA treatment on disease. Physical examination of both animals was carried out at biweekly intervals throughout the study. This examination included palpation of lymph nodes, assessment for potential opportunistic infections, weight measurements, and analysis of blood chemistry and complete blood counts. Chronic diarrhea in both animals completely resolved within the first month of treatment and both animals gained weight, with weights returning to preinfection levels within 4 months (Fig. 4). The 4-month therapeutic regimen, however, failed to completely resolve a preexisting *Mycobacterium* sp. infection in M395, and he was humanely sacrificed. Therapy was continued in the remaining monkey (animal R393) for an additional 2 months and then discontinued. Despite virus rebound after treatment was discontinued, R393 remained clinically asymptomatic until sacrifice.

Toxicity. Serum chemistries and complete blood counts were also analyzed at biweekly intervals during the study, and a complete histopathological examination of the tissues was performed at sacrifice to identify drug-induced toxicity. The mean chemistry values over the period of treatment are shown in Table 1. Other than the low platelet values in monkey R395, who was thrombocytopenic prior to the onset of therapy, no change in the normal levels of blood components that signal bone, liver, heart, and kidney disease were observed in either animal. Complete blood counts were also within normal range, confirming the lack of drug-induced bone marrow toxicity (data not shown).

Histopathological examination of the organs at necropsy also revealed no evidence of drug toxicity. In particular, the histopathology of the heart was unremarkable, with the cardiovascular tissues in both animals lacking any sign of mononuclear cell infiltrates typical of those found in animals treated with other NRTIs (3) (data not shown). Together, these findings indicate that EFdA at this dose and duration of therapy had no effect on liver, kidney, heart, and bone marrow function.

Virus levels in tissue reservoirs. Even though virus was undetectable in the plasma, virus production within tissues collected

TABLE 1 Effects of EFdA therapy on multiorgan function

Assay	Normal range	Mean values for monkey[a]: R393	R395
Alanine aminotransferase (U/liter)	31–50	23	28
Aspartate transaminase (U/liter)	19–38	38	35
Alkaline phosphatase (U/liter)	55–237	155	175
Bilirubin (mg/dl)	0.1–0.3	0.3	0.03
Blood urea nitrogen (mg/dl)	16–30	19	22
Creatinine (mg/dl)	0.7–1.4	1.2	1.1
Blood urea nitrogen /creatinine (ratio)	10–20	17	20
Albumin (g/dl)	3.2–4.1	4.3	2.9
Platelets (#/dl)	260–361	371	40
Total protein (g/dl)	6.4–7.0	7.3	7.6
Calcium (mg/dl)	8.7–10.9	9.1	8.3
Potassium (mg/dl)	3.3–3.7	4	4.2

[a] Data are from ten tests total.

TABLE 2 Effect of EFdA therapy on SIV expression in tissues

Tissue[a]	Drug effects on monkey: R395 Pre-EFdA (2 months before therapy)	R395 At necropsy (after 4 months therapy)	R393 Day of EFdA stop (after 6 months therapy)	R393 At necropsy (5 months after stopping therapy)
Plasma	3.1×10^4	Undetectable	Undetectable	2.6×10^4
PBMC	5.4×10^4	Undetectable	Undetectable	2.2×10^3
Axillary lymph node	2.7×10^3	8×10^1	NA[b]	1.9×10^5
Pancreas		Undetectable		Undetectable
Spleen		Undetectable		4×10^4
Thymus		Undetectable		Undetectable
Ileum		Undetectable		Undetectable
Tonsil		Undetectable		1.6×10^4
Lung		Undetectable		4.2×10^2
Seminal vesicles		Undetectable		Undetectable
Prostate		Undetectable		Undetectable
Jejunum		Undetectable		4.1×10^1
Mesenteric lymph node		Undetectable		3.5×10^3
Kidney		Undetectable		2.6×10^1
Duodenum	2.7×10^1	Undetectable	Undetectable	1.5×10^1
Colon		Undetectable		4.1×10^1
Liver				1.4×10^1
Cecum				7×10^0

[a] Counts in plasma is measured in copies/ml plasma, and those in the other tissues are measured in copies/250 ng total RNA.
[b] NA, not available.

from both animals by either biopsy during treatment or at necropsy during (R395) or after (R393) treatment was analyzed to determine the impact of EFdA on SIV replication in tissues using primers that amplify full-length genomes as a measure of virus production in susceptible target cells. Not surprisingly, viral RNA was readily detected in most tissues obtained from the monkey (animal R393) that was sacrificed after he rebounded (Table 2), with the highest levels of expression observed in the peripheral lymph nodes and spleen. Interestingly, neither the seminal vesicles nor the prostate of the male reproductive tract contained detectable virus, despite the fact that this animal was sacrificed during the fall breeding season.

In contrast, virus could not be detected in most tissues obtained by biopsy from R393 or at sacrifice of animal R395, both of which were obtained while the animals were undergoing therapy. Analysis of necropsied tissues from R395 showed that SIV RNA could be identified in only one organ, an axillary lymph node, and then only at a level barely exceeding the threshold for detection. Similar results were obtained from PBMC and a duodenal biopsy specimen taken from monkey R393 just prior to stopping treatment. These findings suggest that EFdA is readily distributed among the major organs, including those of the reproductive tract, where it can access susceptible target cells and maintain a persistent block to virus replication.

DISCUSSION

Nucleoside/nucleotide reverse transcriptase inhibitors have proven to be the most effective anti-HIV therapeutics to date (11). Indeed, first-line treatment (highly active antiretroviral therapy; HAART) usually consists of two NRTIs plus another drug from a different class. Not surprisingly, however, despite the potency of these compounds, HIV continues to be refractory from clearance, with strains of HIV resistant to more than one of these drugs now resident in the treatment-naïve population (7, 8). Effective therapy typically also requires high doses (200 to 600 mg daily) that must be taken long term to effectively treat chronic infection. Interest in increasing the repertoire of available drugs thus remains high.

EFdA offers several advantages (9, 13, 14, 15, 16, 17). *In vitro*, it is the most potent anti-HIV compound described to date (15), with an EC_{50} that allows an effective dose that is significantly lower than that of other NRTIs. In this report, we show that EFdA inhibits SIV equally well and, like that observed for HIV-1, is more potent *in vitro* than TFV and FTC. The equivalent potency against both HIV-1 and SIV suggests that EFdA will retain excellent activity against all HIV-1 subtypes, a factor that further highlights its potential importance for global health.

Although the *in vivo* results reported here are confined to a 6-month therapeutic regimen in two macaques taken from another study, the rapid and profound reduction in virus burden observed in both plasma and tissues and the continued efficacy during 4 to 6 months of therapy without measurable toxicity in both animals are encouraging.

One potential concern is that EFdA treatment resulted in selection of RT mutations associated with high-level resistance to the widely used NRTIs lamivudine (3TC) and FTC (23, 25). This finding might discourage the use of EFdA as a first-line therapy, because it might preclude 3TC and FTC from subsequent use in these patients. However, M184I/V mutations are already prevalent in treatment-experienced patients due to the widespread use of both 3TC and FTC in HAART (20, 25). Indeed, despite the appearance of M184V/I-containing variants in the rebounded virus after drug was removed, EFdA successfully controlled virus burden to undetectable levels in both blood and tissues throughout the interval of therapy. Together, these findings provide support for further studies designed to address issues of drug resistance, toxicity, and the presence of viral reservoirs with this compound.

ACKNOWLEDGMENTS

This work was supported by Public Health Service grants AI079801 (M.A.P.), AI076119 (S.G.S.), and AI055944 (M.M.C.) from the National Institutes of Health and a grant-in-aid from Yamasa Corporation, Chiba, Japan.

We gratefully acknowledge Mike Miller, Gilead Biosciences, for supplying TFV and Yamasa Corporation for providing EFdA for these studies.

REFERENCES

1. **Amedee AM, et al.** 1995. Genotypic selection of simian immunodeficiency virus in macaque infants infected transplacentally. J. Virol. **69**: 7982–7990.
2. **Amedee AM, et al.** 1996. Genotypic analysis of infant macaques infected transplacentally and orally. J. Med. Primatol. **25**:225–235.
3. **Annamalai L, et al.** 2010. Myocarditis in CD8-depleted SIV-infected rhesus macaques after short-term dual therapy with nucleoside and nucleotide reverse transcriptase inhibitors. PLoS One **5**:e14429.
4. **Fuller DH, et al.** 2002. Induction of mucosal protection against primary, heterologous simian immunodeficiency virus by a DNA vaccine. J. Virol. **76**:3309–3317.
5. **Fuller DH, et al.** 2006. DNA immunization in combination with effective antiretroviral drug therapy controls viral rebound and prevents simian AIDS after treatment is discontinued. Virology **348**:200–215.
6. **Fuller DH, et al.** 2012. Therapeutic DNA vaccine induces broad T cell responses in the gut and sustained protection from viral rebound and AIDS in SIV-infected rhesus macaques. PLoS One **7**:e33715.

7. **Gagliani LH, et al.** 2011. The association between primary antiretroviral resistance and HAART virologic failure in a developing set. AIDS Res. Hum. Retrovir. **27**:251–256.
8. **Graf T, et al.** 2011. HIV-1 genetic diversity and drug resistance among treatment naive patients from southern Brazil: an association of HIV-1 subtypes with exposure categories. J. Clin. Virol. **51**:186–191.
9. **Hattori S, et al.** 2009. Potent activity of a nucleoside reverse transcriptase inhibitor, 4′-ethynyl-2-fluoro-2′-deoxyadenosine, against HIV-1 infection in Hu-PBMC-NOD/SCID/JAK3null (NOJ) mouse model. Antimicrob. Agents Chemother. **53**:3887–3893.
10. **Ibe S, Sugiura W.** 2011. Clinical significance of HIV reverse-transcriptase inhibitor-resistance mutations. Future Microbiol. **6**:295–315.
11. **Ilina T, Parniak MA.** 2008. HIV-1 reverse transcriptase inhibitors, p 121–167. *In* Jeang KT, et al (ed), HIV-1: molecular biogenesis and pathogenesis: clinical applications, 2nd ed. Advances in pharmacology. Academic Press, New York, NY.
12. **Karim QA, et al.** 2010. Effectiveness and safety of tenofovir gel, an antiretroviral microbicide, for the prevention of HIV infection in women. Science **329**:1168–1174.
13. **Kawamoto A, et al.** 2008. 2′-Deoxy-4′-C-ethynyl-2-halo-adenosines active against drug-resistant human immunodeficiency virus type 1 variants. Int. J. Biochem. Cell Biol. **40**:2410–2420.
14. **Kohgo S, et al.** 2003. Synthesis of 4′-C-ethynyl and 4′-C cyano purine nucleosides from natural nucleosides and their anti-HIV activity. Nucleosides Nucleotides Nucleic Acids **22**:887–889.
15. **Michailidis E, et al.** 2009. Mechanism of inhibition of HIV-1 reverse transcriptase by 4′-ethynyl-2-fluoro-2′-deoxyadenosine triphosphate, a translocation defective reverse transcriptase inhibitor. J. Biol. Chem. **284**: 35681–35691.
16. **Nakata H, et al.** 2007. Antiviral activity against HIV-1, intracellular metabolism, and effects on human DNA polymerases of 4′-ethynyl-2-fluoro-2′-deoxyadenosine. Antimicrob. Agents Chemother. **51**:2701–2708.
17. **Ohrui H, et al.** 2007. 2′-Deoxy-4′-C-ethynyl-2-fluoroadenosine: a nucleoside reverse transcriptase inhibitor with highly potent activity against wide spectrum of HIV-1 strains, favorable toxic profiles, and stability in plasma. Nucleosides Nucleotides Nucleic Acids **26**:1543–1546.
18. **Puthanakit T, et al.** 2010. HIV-1 drug resistance mutations in children after failure of first-line nonnucleoside reverse transcriptase inhibitor-based antiretroviral therapy. HIV Med. **11**:565–572.
19. **Seman AL, Pewen WF, Fresh LF, Martin LN, Murphey-Corb M.** 2000. The replicative capacity of rhesus macaque peripheral blood mononuclear cells for simian immunodeficiency virus in vitro is predictive of the rate of progression to AIDS in vivo. J. Gen. Virol. **81**:2441–2449.
20. **Sukasem C, et al.** 2007. Surveillance of genotypic resistance mutations in chronic HIV-1 treated individuals after completion of the national access to antiretroviral program in Thailand. Infection **35**:81–88.
21. **Taber R, et al.** 2006. Effects of monotherapy with (R)-9-(2-phosphonylmethoxypropyl)adenine (PMPA) on the evolution of a primary simian immunodeficiency virus (SIV) isolate. Virology **354**:116–131.
22. **Trichel AM, et al.** 1997. SIV/DeltaB670 transmission across oral, colonic, and vaginal mucosae in the macaque. J. Med. Primatol. **26**:3–10.
23. **Van Rompay KK, et al.** 2002. Virulence and reduced fitness of simian immunodeficiency virus with the M184V mutation in reverse transcriptase. J. Virol. **76**:6083–6092.
24. **Van Rompay KK, et al.** 2007. Sequential emergence and clinical implications of viral mutants with K70E and K65R mutation in reverse transcriptase during prolonged tenofovir monotherapy in rhesus macaques with chronic RT-SHIV infection. Retrovirology **4**:25.
25. **Westin MR, et al.** 2011. Resistance-associated mutation prevalence according to subtypes B and non-B of HIV type 1 in antiretroviral-experienced patients in Minas Gerais, Brazil. AIDS Res. Hum. Retrovir. **27**:981–987.

Bioorganic & Medicinal Chemistry Letters 22 (2012) 2308–2311

Contents lists available at SciVerse ScienceDirect

Bioorganic & Medicinal Chemistry Letters

journal homepage: www.elsevier.com/locate/bmcl

Substituent effects on P2-cyclopentyltetrahydrofuranyl urethanes: Design, synthesis, and X-ray studies of potent HIV-1 protease inhibitors

Arun K. Ghosh [a,*], Bruno D. Chapsal [a], Melinda Steffey [a], Johnson Agniswamy [b], Yuan-Fang Wang [b], Masayuki Amano [c], Irene T. Weber [b], Hiroaki Mitsuya [c,d]

[a] Department of Chemistry and Department of Medicinal Chemistry, Purdue University, West Lafayette, IN 47907, USA
[b] Department of Biology, Molecular Basis of Disease, Georgia State University, Atlanta, GA 30303, USA
[c] Departments of Hematology and Infectious Diseases, Kumamoto University Graduate School of Medical and Pharmaceutical Sciences, Kumamoto 860-8556, Japan
[d] Experimental Retrovirology Section, HIV and AIDS Malignancy Branch, National Cancer Institute, National Institutes of Health, Bethesda, MD 20892, USA

ARTICLE INFO

Article history:
Received 28 December 2011
Accepted 17 January 2012
Available online 2 February 2012

Keywords:
HIV-1 protease inhibitors
P2 ligand
Drug resistance
Design and synthesis
X-ray crystal structure

ABSTRACT

The design, synthesis, and biological evaluation of novel C3-substituted cyclopentyltetrahydrofuranyl (Cp-THF)-derived HIV-1 protease inhibitors are described. Various C3-functional groups on the Cp-THF ligand were investigated in order to maximize the ligand-binding site interactions in the flap region of the protease. Inhibitors **3c** and **3d** have displayed the most potent enzyme inhibitory and antiviral activity. Both inhibitors have maintained impressive activity against a panel of multidrug resistant HIV-1 variants. A high-resolution X-ray crystal structure of **3c**-bound HIV-1 protease revealed a number of important molecular insights into the ligand-binding site interactions.

HIV-1 protease inhibitors continue to be a critical component of frontline therapy in the treatment of HIV patients.[1–3] Our continuing studies on the structure-based design of inhibitors targeting the protein backbone led to the discovery of a variety of novel HIV-1 protease inhibitors (PIs) with broad-spectrum activity against multidrug-resistant HIV-1 variants.[4–8] We recently reported various C3-functionalized cyclopentyltetrahydrofuran (Cp-THF)-derived P2-ligands designed to specifically interact with the flap Gly48 amide NH in the S2-subsite of the HIV-1 protease.[9] One of these inhibitors, **2** (Fig. 1), containing a 3-(*R*)-hydroxy group on the Cp-THF core displayed exceptionally potent enzyme inhibitory (K_i = 5 pM) and antiviral activity (IC_{50} = 2.9 nM). This inhibitor also exhibited potent activity against a panel of multidrug-resistant HIV-1 variants. The X-ray crystal structure of **2**-bound HIV protease revealed an extensive hydrogen-bonding network with the enzyme backbone.[9] Of particular interest, the 3-(*R*)-hydroxy group of the Cp-THF ligand was involved in an interesting water-mediated interaction with the backbone NH amide bond of Gly48. This specific interaction was not present in inhibitor **1**. These additional interactions observed with **2** may have contributed toward its impressive drug resistance profile. [9]

Based upon the **2**-bound X-ray crystal structure of HIV-1 protease, and given the significant gain in antiviral activity observed with the addition of C3-polar substituents on the Cp-THF P2 ligand, we subsequently speculated that N-substituted functionalities, particularly *N*-acyl, *N*-carbamate or *N*-sulfonyl derivatives could function as both a hydrogen-bonding donor and acceptor. The NH proton could conceivably form an effective hydrogen bond with the proximal Gly48 carbonyl while amide or urethane carbonyl oxygen may form an additional interaction with the protease backbone. Indeed, our previous exploration of such hydrogen bond donor and acceptor functionalities on P2-ligand frameworks led to remarkably potent HIV-1 protease inhibitors with broad-spectrum antiviral activity. [4–9] Herein, we report the design, synthesis and biological evaluation of a series of HIV-1 protease inhibitors with C-3 substituted Cp-THF as the P2-ligand. A number of inhibitors exhibited exceptionally potent antiviral activity against a panel of multidrug-resistant HIV-1 variants. A protein-ligand X-ray crystal structure also provided important molecular insight into the ligand-binding site interactions.

The synthesis of ligands containing various N-substituents with either stereochemistry at C3 was accomplished starting from our previously reported optically active ketone intermediate **4**[10] as shown in Scheme 1. Ketone **4** was converted to methyloxime derivatives **5** in 96% yield. Reduction of **5** with a mixture of Pd/C and Raney-Ni under hydrogen pressure (80 psi) provided the corresponding amine as a 3:1 diastereomeric mixture.[11] The amine mixture was reacted with Ac_2O in the presence of Et_3N and a catalytic amount of DMAP to yield a mixture of isomeric TBS-protected

* Corresponding author. Tel.: +1 765 494 5323; fax: +1 765 496 1612.
E-mail address: akghosh@purdue.edu (A.K. Ghosh).

0960-894X/$ - see front matter © 2012 Elsevier Ltd. All rights reserved.
doi:10.1016/j.bmcl.2012.01.061

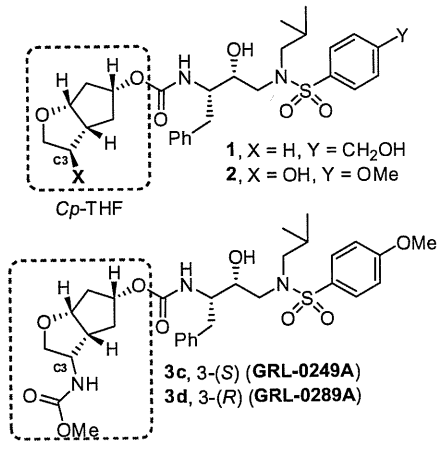

Figure 1. Structure of protease inhibitors **1,2, 3c–d.**

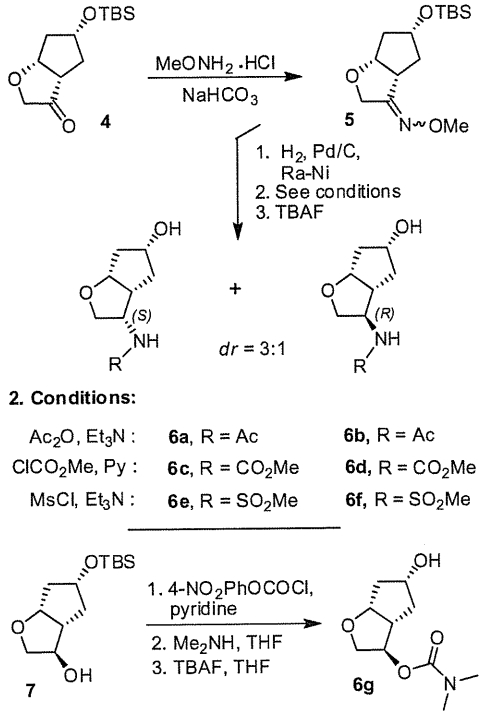

Scheme 1. Synthesis of C3-substituted ligands **6a–g.**

amide intermediates in 80% yield. Treatment of the respective amides with TBAF in THF and chromatographic separation furnished diastereomerically pure ligands **6a** and **6b** in excellent yield. Similarly, the amine mixture was treated with methyl chloroformate and pyridine, or mesyl chloride and Et_3N to afford the corresponding carbamates and sulfonamides. Treatment of the respective crude mixtures with TBAF in THF followed by chromatographic separation afforded diastereoisomeric *N*-carbamate ligands **6c** and **6d**, and *N*-mesyl ligands **6e** and **6f**, respectively. The assignment of stereochemistry on the ligands was carried out by NOE or NOESY experiments of the corresponding mixed activated carbonates **8a**, **8c**, and **8e**. To probe the importance of the free NH, we have synthesized ligand **6g** containing a 3-(*R*)-*O*-dimethylaminocarbamate group. This was synthesized in three consecutive steps starting from our previously reported optically active alcohol **7**.[9] Treatment of **7** with 4-nitrophenyl chloroformate in the presence of pyridine furnished the corresponding mixed activated carbonate. The resulting carbonate was reacted with a bubbling stream of

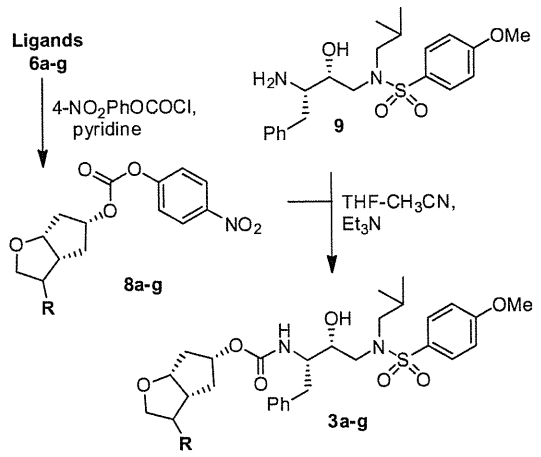

Scheme 2. Synthesis of protease inhibitors **3a–g.**

Me_2NH gas to provide the corresponding TBS-protected ligand. Removal of the TBS-group with TBAF furnished ligand **6g** in excellent yield.

For the synthesis of HIV protease inhibitors, all ligand alcohols **6a–g** were reacted with 4-nitrophenyl chloroformate in the presence of pyridine in CH_2Cl_2 to furnish the corresponding mixed activated carbonates **8a–g** (Scheme 2).[9,10] The activated carbonates were then reacted with previously reported hydroxyethylamine isostere **9**[9] in the presence of Et_3N in THF/CH_3CN for 2–4 days to give corresponding inhibitors **3a–g**.

Inhibitors **3a–g** were initially tested in enzyme inhibitory assays using the method developed by Toth and Marshall,[12] and then evaluated for in vitro antiviral assays. Results are shown in Table 1. All inhibitors displayed impressive inhibitory potency and high antiviral activity. Inhibitors **3a** and **3b** that, contain a 3-(*S*)- or 3-(*R*)-*N*-acetyl substituent on the Cp-THF ligand, exhibited similar potency (7.4 and 7.5 pM, respectively). Interestingly, the stereochemistry at C3 seemed to have little effect. Inhibitor **3c** with a 3-(*S*)-*N*-methoxycarbonyl displayed the most impressive enzyme and antiviral potency (K_i = 1.8 pM and IC_{50} = 1.6 nM). The isomeric inhibitor **3d** provided slightly lower potency. Inhibitors **3e** and **3f** that contain a 3-*N*-mesyl on the Cp-THF ligand, showed a substantial reduction in activity probably due to the increase in steric bulk created by the *N*-mesyl group. Inhibitor **3g** that contains an O-substituted dimethylaminocarbamate in place of N-substituted carbamate at C3 provided a good antiviral activity, similar to that of **3d**.

Inhibitors **3c** and **3d**, were further evaluated against a panel of multidrug-resistant (MDR) HIV-1 variants and their antiviral activities were compared to clinically available PI, darunavir (DRV).[6,13] Results are shown in Table 2. All inhibitors exhibited low nanomolar EC_{50} values against the wild-type HIV-$1_{ERS104pre}$ laboratory strain, isolated from a drug-naïve patient.[13] Inhibitor **3d** had the most potent activity (EC_{50} = 3 nM) similar to that of DRV. When tested against a panel of multidrug-resistant HIV-1 strains, the EC_{50} of **3d** remained in the low nanomolar value range (15–24 nM) and its fold-changes in activity were similar to those observed with DRV.[6,13] Interestingly, inhibitor **3c**, with the opposite (*S*) stereochemistry at C3, displayed slightly lower antiviral activities against all viral strains compared to **3d**. However, the fold-changes in EC_{50} for **3c** remained low (<3) against all MDR HIV-1 viruses. The fold-changes contrasted with those of **3d** and even DRV, for which the respective EC_{50}'s increased by a factor of at least three against the MDR viruses examined.[14]

In order to gain molecular insights on the ligand-binding site interactions responsible for the potent activity and excellent resistance profile of **3c**, we have determined the X-ray crystal structure

Table 1
Structures and potency of inhibitors **3a–g**[a]

Entry	Inhibitor structure	K_i (pM)	IC_{50} (nM)[b]
1	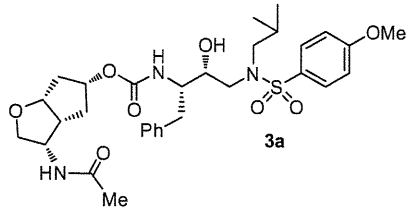 **3a**	7.4	25
2	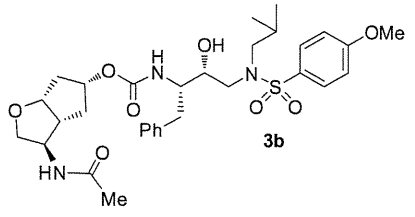 **3b**	7.5	31
3	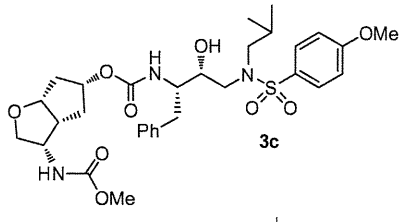 **3c**	1.8	1.6
4	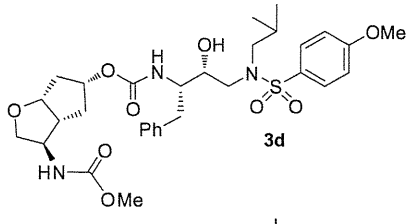 **3d**	4.0	4.6
5	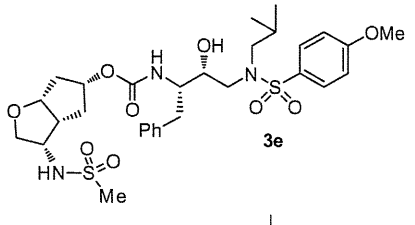 **3e**	32	28
6	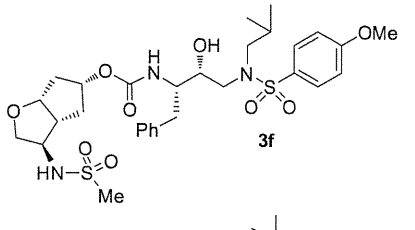 **3f**	180	50
7	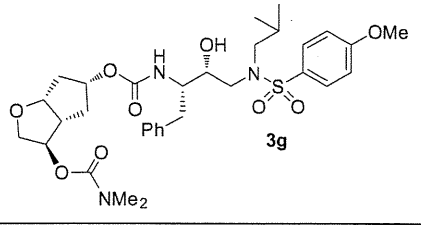 **3g**	20	4.7

[a] Values are the mean value of at least two experiments.
[b] Human T-lymphoid (MT-2) cells (2×10^3) were exposed to 100 $TCID_{50}$ of HIV-1_{LAI} and cultured in the presence of each PI, and IC_{50} values were determined using the MTT assay. The IC_{50} values of amprenavir (APV), saquinavir (SQV), indinavir (IDV), and darunavir (DRV) were 0.03, 0.015, 0.03, and 0.003 μM, respectively.

Table 2
Comparison of the antiviral activity of **3c**, **3d**, and DRV against multidrug-resistant HIV-1 variants

Virus[a]	EC_{50} (μM) ±SDs, (fold-change)[b]		
	3c	**3d**	**DRV**
HIV-$1_{ERS104pre}$ (wt)	0.029 ± 0.002	0.003 ± 0.001	0.004 ± 0.001
HIV-$1_{MDR/B}$ (X4)	0.075 ± 0.011 (3)	0.018 ± 0.003 (6)	0.019 ± 0.006 (5)
HIV-$1_{MDR/C}$ (X4)	0.030 ± 0.006 (1)	0.015 ± 0.005 (5)	0.011 ± 0.003 (3)
HIV-$1_{MDR/G}$ (X4)	0.039 ± 0.001 (1)	0.020 ± 0.005 (7)	0.011 ± 0.002 (3)
HIV-$1_{MDR/TM}$ (X4)	0.074 ± 0.006 (3)	0.024 ± 0.004 (8)	0.028 ± 0.001 (7)

[a] Amino acid substitutions identified in the protease-encoding region of HIV-$1_{ERS104pre}$, HIV-$1_{MDR/B}$, HIV-$1_{MDR/C}$, HIV-$1_{MDR/G}$, HIV-$1_{MDR/TM}$ compared to the consensus type B sequence cited from the Los Alamos database include L63P in HIV-$1_{ERS104pre}$; L10I, K14R, L33I, M36I, M46I, F53I, K55R, I62V, L63P, A71V, G73S, V82A, L90M, I93L in HIV-$1_{MDR/B}$; L10I, I15V, K20R, L24I, M36I, M46L, I54V, I62V, L63P, K70Q, V82A, and L89M in HIV-$1_{MDR/C}$; L10I, V11I, T12E, I15V, L19I, R41K, M46L, L63P, A71T, V82A, and L90M in HIV-$1_{MDR/G}$; L10I, K14R, R41K, M46L, I54V, L63P, A71V, V82A, L90M, I93L in HIV-$1_{MDR/TM}$. HIV-$1_{ERS104pre}$ served as a source of wild-type HIV-1.
[b] EC_{50} values were determined by using PHA-PBMs as target cells and the inhibition of p24 Gag protein production for each drug was used as an endpoint. The numbers in parentheses represent the fold-change in EC_{50} values for each isolate compared to the EC_{50} values for the wild-type HIV-$1_{ERS104pre}$. All assays were conducted in duplicate, and the data shown represent mean values (±1 standard deviations) derived from the results of two or three independent experiments. PHA-PBMs were derived from a single donor in each independent experiment. DRV (darunavir).

of the HIV wild-type protease complexed with **3c** (Fig. 2).[15] The structure was refined to an R-factor of 14.9% and a resolution of 1.23 Å. The inhibitor is bound to the protease dimer in two orientations related by a 180° rotation, with a 50/50 relative occupancy. The protease backbone structure showed a very low rms deviation of 0.11 Å for all Cα carbons compared to the protease complexes of **2**[9] or DRV.[21] As shown in Figure 2, the inhibitor interactions in the protease binding site extend from S2 to S2′ protease subsites and consist of a series of strong hydrogen bonds and weaker C–H···O and C–H···π interactions similar to those previously described for DRV,[21] or inhibitor **2**.[9] The Cp-THF cyclic oxygen forms a strong hydrogen bond with the backbone amide NH of Asp29 in the protease S2-binding site, similar to that previously observed with other Cp-THF-based inhibitors **1**[5] and **2**.[9] Critical differences, however, are observed with the additional interactions that the 3-(*S*)-*N*-methoxycarbonyl amino substituent on the Cp-THF makes throughout the S2–S3 subsites. As shown in Figure 2, the carbamate NH forms a strong hydrogen bond with the Gly48 backbone carbonyl. The carbamate carbonyl is observed to interact with the Arg8′ guanidine side chain through a conserved water molecule. The methyl of the methoxy group then fits within the S3-hydrophobic pocket. The C3-*N*-methoxycarbonyl amino group creates a network of tight hydrogen bonds that literally links the protease flap region to the S2–S3 subsites' dimer interface. These new interactions and enthalpic nature of the additional hydrogen bonding created by the P2-ligand may certainly exert an enhanced anchoring effect of the inhibitor into the S2-subsite and further stabilize the closed conformation of the protease–ligand complex.

In conclusion, we have reported the structure-based design of a series of highly potent HIV-1 protease inhibitors incorporating C3-substituted cyclopentyltetrahydrofuranyl urethanes as P2-ligands. Various C3-*N*-substituents were investigated in order to create multiple interactions in the S2-subsite of the protease and specifically with the protease flap region. Inhibitors **3c** and **3d** displayed remarkable inhibitory potency and antiviral activity. When tested against a panel of MDR HIV-1 strains, inhibitor **3d**, with a 3-(*R*)-methoxycarbonyl on the Cp-THF ligand, provided the most impressive EC_{50}s and fold-changes in activity which are comparable to those observed with clinically available DRV. Isomeric inhibitor **3c** displayed lower antiviral activity. However, it exhibited strikingly low fold-changes of antiviral activity when tested against MDR HIV-1 viruses. An X-ray crystal structure of the protease–**3c**

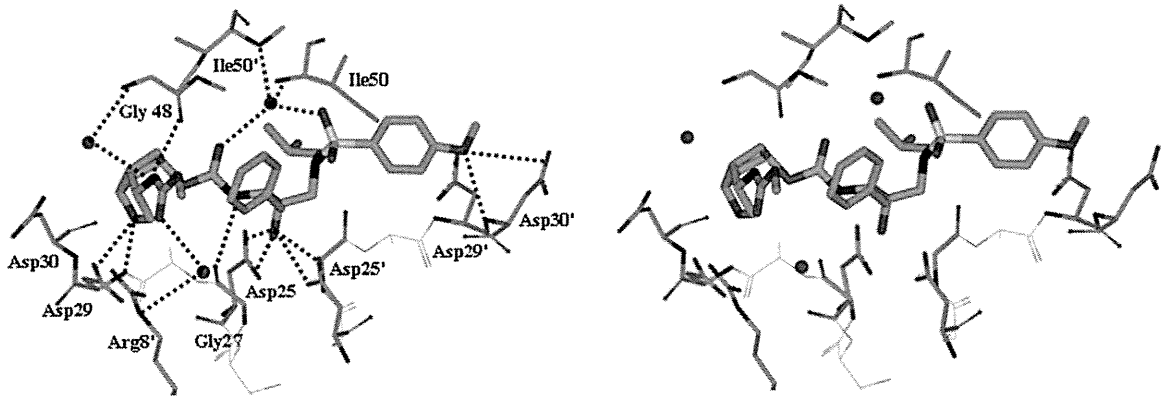

Figure 2. Stereoview of the X-ray structure of inhibitor **3c** (green)-bound HIV-1 protease (PDB code: 4DFG). All strong hydrogen bonding interactions are shown as dotted lines.

complex was determined at a 1.23 Å resolution. Inhibitor **3c** made extensive interactions throughout the protease binding site. The complex network of hydrogen-bonding interactions created by the *N*-methyl carbamate substituent in addition to those created by the isostere in the protease active site may account for the impressive antiviral activity and superb resistance profile observed with inhibitor **3c**. Further designs along this line and ligand optimization are currently underway.

Acknowledgements

This research was supported by the National Institutes of Health (Grant GM53386 to A.K.G. and Grant GM62920 to I.T.W.). This work was also supported by the Intramural Research Program of the Center for Cancer Research, National Cancer Institute, National Institutes of Health, and in part by a Grant-in-Aid for Scientific Research (Priority Areas) from the Ministry of Education, Culture, Sports, Science, and Technology of Japan (Monbu Kagakusho), a Grant for Promotion of AIDS Research from the Ministry of Health, Welfare, and Labor of Japan, and the Grant to the Cooperative Research Project on Clinical and Epidemiological Studies of Emerging and Reemerging Infectious Diseases (Renkei Jigyo) of Monbu-Kagakusho.

References and notes

1. Conway, B. *Future Virol.* **2009**, *4*, 39.
2. Hue, S.; Gifford, R. J.; Dunn, D.; Fernhill, E.; Pillay, D. *J. Virol.* **2009**, *83*, 2645.
3. Little, S. J.; Holte, S.; Routy, J. P.; Daar, E. S.; Markowitz, M.; Collier, A. C.; Koup, R. A.; Mellors, J. W.; Connick, E.; Conway, B.; Kilby, M.; Wang, L.; Whitcomb, J. M.; Hellmann, N. S.; Richman, D. D. N. *Engl. J. Med.* **2002**, *347*, 385.
4. Ghosh, A. K. *J. Med. Chem.* **2009**, *52*, 2163.
5. Ghosh, A. K.; Sridhar, P. R.; Leshchenko, S.; Hussain, A. K.; Li, J.; Kovalevsky, A. Y.; Walters, D. E.; Wedekind, J. E.; Grum-Tokars, V.; Das, D.; Koh, Y.; Maeda, K.; Gatanaga, H.; Weber, I. T.; Mitsuya, H. *J. Med. Chem.* **2006**, *49*, 5252.
6. Ghosh, A. K.; Dawson, Z. L.; Mitsuya, H. *Bioorg. Med. Chem. Lett.* **2007**, *15*, 7576.
7. Ghosh, A. K.; Leshchenko-Yashchuk, S.; Anderson, D. D.; Baldridge, A.; Noetzel, M.; Miller, H. B.; Tie, Y. F.; Wang, Y. F.; Koh, Y.; Weber, I. T.; Mitsuya, H. *J. Med. Chem.* **2009**, *52*, 3902.
8. Ghosh, A. K.; Chapsal, B. D.; Weber, I. T.; Mitsuya, H. *Acc. Chem. Res.* **2008**, *41*, 78.
9. Ghosh, A. K.; Chapsal, B. D.; Parham, G. L.; Steffey, M.; Agniswamy, J.; Wang, Y.-F.; Amano, M.; Weber, I. T.; Mitsuya, H. *J. Med. Chem.* **2011**, *54*, 5890.
10. Ghosh, A. K.; Chapsal, B. D.; Baldridge, A.; Ide, K.; Koh, Y.; Mitsuya, H. *Org. Lett.* **2008**, *10*, 5135.
11. Li, J. J.; Sutton, J. C.; Nirschl, A.; Zou, Y.; Wang, H.; Sun, C.; Pi, Z.; Johnson, R.; Krystek, S. R.; Seethala, R.; Golla, R.; Sleph, P. G.; Beehler, B. C.; Grover, G. J.; Fura, A.; Vyas, V. P.; Li, C. Y.; Gougoutas, J. Z.; Galella, M. A.; Zahler, R.; Ostrowski, J.; Hamann, L. G. *J. Med. Chem.* **2007**, *50*, 3015.
12. Toth, M. V.; Marshall, G. R. *Int. J. Pept. Protein Res.* **1990**, *36*, 544.
13. Koh, Y.; Nakata, H.; Maeda, K.; Ogata, H.; Bilcer, G.; Devasamudram, T.; Kincaid, J. F.; Boross, P.; Wang, Y.-F.; Tie, Y.; Volarath, P.; Gaddis, L.; Harrison, R. W.; Weber, I. T.; Ghosh, A. K.; Mitsuya, H. *Antimicrob. Agents Chemother.* **2003**, *47*, 3123.
14. Ghosh, A. K.; Chapsal, B. Mitsuya, H. In *Aspartic Acid Proteases as Therapeutic Targets*; Ghosh, A., Ed.; Wiley-VCH Verlag GmbH & Co. KGaA: Weinheim, 2010; pp 245–262.
15. The protein-ligand X-ray structure of **3c**-bound HIV-1 protease will be deposited in PDB (PDB ID: 4DFG). The HIV-1 protease was expressed and purified as previously described.[16] The protease–inhibitor complex was crystallized at room temperature by the hanging drop vapor diffusion method with well solutions of 1.2 M ammonium chloride and 0.1 M sodium acetate buffer (pH 4.8). Diffraction data were collected on a single crystal cooled to 90 K at SER-CAT BM beamline 22, Advanced Photon Source, Argonne National Laboratory (Chicago, IL, U.S.), with an X-ray wavelength of 1.0 Å and processed by HKL-2000 with R_{merge} of 7.2%. The PR structure was used in molecular replacement by PHASER[17] in the CCP4i suite[18] and refined to 1.45 Å resolution using SHELX-97 and COOT[19] for manual modification. PRODRG-2[20] was used to construct the inhibitor and the restraints for refinement. Alternative conformations were modeled, anisotropic atomic displacement parameters (*B* factors) were applied for all atoms including solvent molecules, and hydrogen atoms were added in the final round of refinement. The final refined solvent structure comprised two Cl^- ions and 142 water molecules.
16. Mahalingam, B.; Louis, J. M.; Hung, J.; Harrison, R. W.; Weber, I. T. *Proteins* **2001**, *43*, 455.
17. Shen, C.-H.; Wang, Y.-F.; Kovalevsky, A. Y.; Harrison, R. W.; Weber, I. T. *FEBS J.* **2010**, *277*, 3699.
18. Potterton, E.; Briggs, P.; Turkenburg, M.; Dodson, E. A. *Acta Crystallogr. Sect. D: Bio. Crystallogr.* **2003**, *59*, 1131.
19. Emsley, P.; Cowtan, K. *Sect. D: Bio. Crystallogr.* **2004**, *60*, 2126.
20. Schuttelkopf, A. W.; van Aalten, D. M. F. *Acta Crystallogr. Sect. D: Bio. Crystallogr.* **2004**, *60*, 1355.
21. Kovalevsky, A. Y.; Liu, F.; Leshchenko, S.; Ghosh, A. K.; Louis, J. M.; Harrison, R. W.; Weber, I. T. *J. Mol. Biol.* **2006**, *363*, 161.

Backbone Binding

DOI: 10.1002/anie.201102762

Enhancing Protein Backbone Binding—A Fruitful Concept for Combating Drug-Resistant HIV**

Arun K. Ghosh, David D. Anderson, Irene T. Weber, and Hiroaki Mitsuya*

Keywords:
antiviral agents · backbone binding · drug resistance · enzymes · proteins

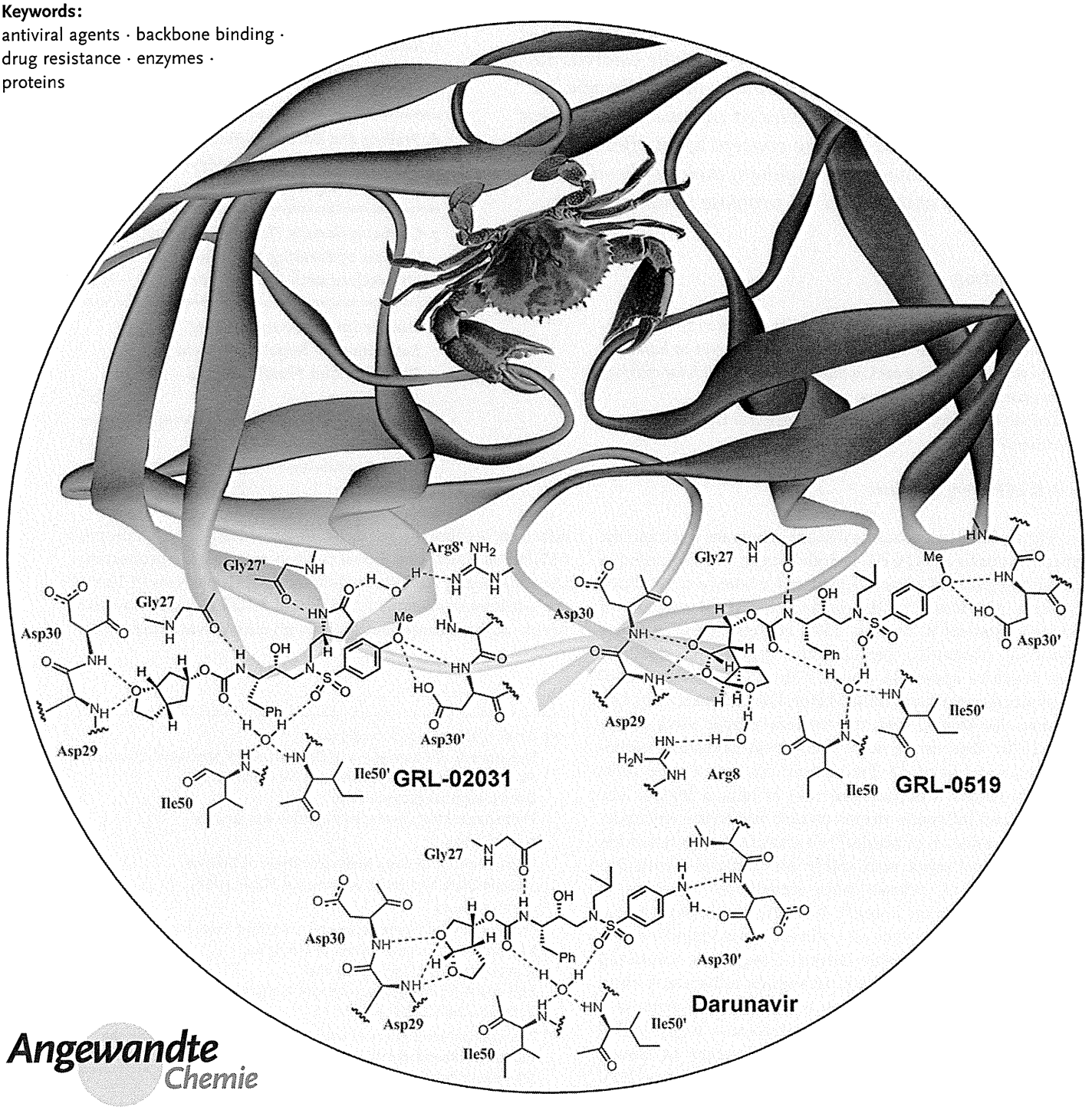

The evolution of drug resistance is one of the most fundamental problems in medicine. In HIV/AIDS, the rapid emergence of drug-resistant HIV-1 variants is a major obstacle to current treatments. HIV-1 protease inhibitors are essential components of present antiretroviral therapies. However, with these protease inhibitors, resistance occurs through viral mutations that alter inhibitor binding, resulting in a loss of efficacy. This loss of potency has raised serious questions with regard to effective long-term antiretroviral therapy for HIV/AIDS. In this context, our research has focused on designing inhibitors that form extensive hydrogen-bonding interactions with the enzyme's backbone in the active site. In doing so, we limit the protease's ability to acquire drug resistance as the geometry of the catalytic site must be conserved to maintain functionality. In this Review, we examine the underlying principles of enzyme structure that support our backbone-binding concept as an effective means to combat drug resistance and highlight their application in our recent work on antiviral HIV-1 protease inhibitors.

From the Contents

1. Introduction 1779

2. Targeting the Protein Backbone to Combat Drug Resistance 1781

3. Structure-Based Design Targeting the Protein Backbone 1783

4. Backbone-Binding Strategy Leading to the Clinical Development of Darunavir to Combat Drug Resistance 1786

5. Retaining Backbone Binding and Designing Exceptionally Potent Bis-THF-Derived PIs 1788

6. Probing the Backbone-Binding Concept as a Design Strategy to Combat Drug Resistance 1792

7. Conformationally Flexible P2 Ligands Capable of Forming Extensive Interactions with the Backbone 1796

8. Further Improvement of Drug Resistance by Targeting Protein Backbone and Protein–Ligand Interactions 1798

9. Summary and Outlook 1799

1. Introduction

> "*It has taken half a century for the selection of antibiotic-resistant bacteria to represent a widespread threat to humans, and yet it takes only weeks to months to select inhibitor-resistant immunodeficiency viruses in treated patients.*"
>
> Esteban Domingo, Christof Biebricher, Manfred Eigen, and John Holland[1]

1.1. A Brief History of Viruses

Viruses have been causing disease in humans since ancient times.[2] As early as 1150 B.C., viral diseases were recorded in the hieroglyphics of ancient Egypt and evidence of smallpox infection was found in the pockmark-scarred remains of Pharaoh Ramses V. In the 15th century, early writings describing preventive inoculations against the smallpox virus began to appear in China.[3] However, it wasn't until the pioneering work of Adolf Mayer, Dimitri Ivanovsky, and Martinus Beijerinck, with the tobacco mosaic virus in the early 1900s, that viruses were recognized as distinct pathogenic microorganisms.[4] Throughout history, viruses have primarily played a detrimental role in human health. The smallpox and influenza viruses caused worldwide epidemics resulting in millions of deaths.[5] To prevent the spread of the aphthovirus pathogen responsible for foot-and-mouth disease, millions of animals were slaughtered resulting in significant economical losses.[6] Recently, the SARS coronavirus made headlines when an outbreak spread rapidly across the world in near-pandemic fashion killing 11% of infected individuals.[7] Also, the highly pathogenic influenza A virus, subtype *H5N1*, often known as avian influenza virus, is a potential pandemic threat and has become a major global concern.[8] The world witnessed the emergence of human immunodeficiency virus (HIV) in the 1980s. Since then, HIV infection leading to acquired immunodeficiency syndrome (AIDS) has become a global crisis of catastrophic proportion infecting nearly 2.6 million new individuals per year.[9] There are effective treatments for HIV and AIDS that can slow the course of the disease, but there is no cure or vaccine to date.

[*] Dr. A. K. Ghosh, D. D. Anderson
Department of Chemistry and Department of Medicinal Chemistry
Purdue University, West Lafayette, IN 47907 (USA)
E-mail: akghosh@purdue.edu
Homepage: http://www.chem.purdue.edu/ghosh/
Dr. I. T. Weber
Department of Biology, Molecular Basis of Disease
Georgia State University, Atlanta, GA 30303 (USA)
Dr. H. Mitsuya
Departments of Hematology and Infectious Diseases
Kumamoto University School of Medicine
Kumamoto 860-8556 (Japan) and
HIV and AIDS Malignancy Branch, National Cancer Institute
Bethesda, MD 20892 (USA)

[**] The frontispiece depicts a "molecular crab" tightly gripping the protein backbone of HIV-1 protease. We thank Dr. Xiaoming Xu for his help in creating this artwork.

1.2. HIV Emergence

The HIV time line began early in 1981 and the virus was first isolated in 1983.[10,11] Since then, millions of individuals throughout the world have been infected with HIV. The resulting onset of AIDS has swept across the continents causing an estimated 25 million deaths and leaving millions of children orphaned.[9] Recent estimates from the joint United Nations program on HIV/AIDS (UNAIDS) indicate that worldwide, over 33 million adults and children are currently living with the disease and 1.8 million AIDS-related deaths occur each year.[9] While these statistics are alarming, significant advancements in both HIV treatment and prevention have appeared to be turning the tide in the fight against AIDS, as evidenced by the steadily decreasing number of annual deaths.[9] Intensive research into the development of novel antiviral agents and the use of multidrug combination therapies have resulted in a significant increase in life expectancy for those with access to therapy.[12,13] Unfortunately, the rapid emergence of drug resistance has rendered many treatments ineffective and continues to be a formidable challenge for molecular design and drug discovery.[14,15] Moreover, the consequences of drug resistance may unravel the progress made toward HIV/AIDS management. Today, there is still an urgent need for the development of novel anti-HIV therapeutics and drug-design tools for combating drug resistance.

1.3. The Advent of Protease Inhibitors

Biochemical events critical to HIV replication have suggested a number of drug-design targets for therapeutic intervention. Among them, the HIV protease enzyme was quickly recognized as an important therapeutic target.[16] It has been demonstrated that an effective HIV protease is essential to the production of mature, infectious HIV virions.[17] Logically, inhibition of the HIV protease became the subject of much pharmaceutical research. Subsequent drug-development efforts led to the advent of the first generation of protease inhibitors (PIs) marking a new era in AIDS chemotherapy.[18] The use of PIs in combination with reverse transcriptase inhibitors proved to be an extremely effective treatment regimen which suppresses viral reproduction and reduces the possibility of viral mutations.[19] Despite their early success, PIs were plagued with several drawbacks including low metabolic stability, poor bioavailability, debilitating side effects, and drug toxicity.[20] Perhaps the most concerning obstacle has been the rapid development of drug-resistant viral strains which render the PIs ineffective.[21] Currently, 40–50% of the patients who achieve initial viral suppression will eventually experience treatment failure.[22] Additionally, these drug-resistant viral strains can be transmitted to new individuals.[23] Success in the future management of HIV/AIDS depends on the development of new antiviral agents that maintain efficacy against drug-resistant viral strains.

Arun K. Ghosh received his BS and MS in Chemistry from the University of Calcutta and Indian Institute of Technology, Kanpur, respectively. He obtained his PhD in 1985 at the University of Pittsburgh. He pursued postdoctoral research with Professor E. J. Corey at Harvard University (1985–1988). He was a research fellow at Merck Research Laboratories prior to joining the University of Illinois-Chicago as an Assistant Professor in 1994. In 2005 he moved to Purdue University, where he is currently the Ian P. Rothwell Distinguished Professor in Chemistry and Medicinal Chemistry. His research interests are in the areas of organic, bioorganic, and medicinal chemistry.

Irene T. Weber received her BS and MS from Cambridge University (UK) and obtained her PhD in 1978 from Oxford University (UK). She pursued postdoctoral research with Professor Thomas Steitz at Yale University. In 1991 she accepted a position as Professor of Microbiology and Immunology at Thomas Jefferson University in Philadelphia. In 2001 she moved to Georgia State University, Atlanta, where she is Professor of Biology and Chemistry and Georgia Cancer Coalition Distinguished Cancer Scientist. Her research focuses on the structure and activity of enzymes.

David Anderson received his BS in chemistry from the University of Wisconsin-Madison. He joined Eli Lilly and Co. in 2001 as an analytical chemist supporting the commercial process development of clinical drug candidates. In 2005 he received his MS from Indiana University-Purdue University at Indianapolis and later moved to Purdue University to study medicinal chemistry with Professor Ghosh. His research focuses on the design and synthesis of HIV-1 protease inhibitors and the total synthesis of pladienolide B.

Hiroaki Mitsuya received his MD and PhD from National Kumamoto University School of Medicine, Japan. In 1982 following training in oncology/hematology/immunology, he joined the National Cancer Institute in Bethesda, Maryland (USA), where he has been Principal Investigator & Chief of the Experimental Retrovirology Section since 1991. Since 1997, he has also served as Professor of Medicine and Chairman of the Departments of Hematology, Clinical Immunology/Rheumatology, and Infectious Diseases at the Kumamoto University School of Medicine.

1.4. Mechanism of Drug Resistance

HIV-1 has an astonishing capacity for genetic evolution which is a major driving force for drug resistance. Its relentless ability to mutate arises from a high mismatch error rate (10^{-3} to 10^{-5} nucleotide bases per cycle) of the virus's reverse transcriptase enzyme and the absence of exonuclease-based proofreading activity.[24,25] These factors, in conjunction with the virus's rapid replication cycle (10^{10} virions per day) and genetic recombination ability, result in seemingly endless genetic diversification.[26,27] However, the number of variants within the quasi-species at a given time is limited by natural selection, deleterious mutations, and limited host cell availability, and by inactivation from the host's immune system response.[28] As a result, the virus population primarily consists of single-mutation strains and relatively few double-mutation strains. Antiretroviral treatment creates a new selection pressure resulting in the amplification of drug-resistant strains. Viral evolution continues over time adding new mutations that restore viral fitness while maintaining drug resistance. This leads to a resurgence of the viral load and eventually treatment failure. Combating drug resistance remains a formidable challenge that must be considered during the design of new antiretroviral agents.

It may be more effective to develop therapies that limit the emergence or growth of HIV-1 variants than to combat these variants once they have already evolved. The development of new classes of antiretroviral drugs with new mechanisms of action, showing durable effects, and causing minimal side effects, are important therapeutic objectives. There is reason to be optimistic as tremendous progress has been made in terms of new drugs which are very potent and with a high genetic barrier to resistance. Recently a number of new approved drugs with novel mechanisms of action, including an integrase inhibitor,[29] and a virus-entry inhibitor,[30] have shown efficacy against resistant strains. However, these drugs quickly succumb to the development of resistance rendering them ineffective.[31,32] Also, maturation inhibition and small-molecule inhibition of HIV pre-mRNA splicing holds considerable promise.[33,34]

1.5. Protease Evolution in Response to Inhibitor Pressure

The evolution of HIV protease in response to therapeutic pressures has been reviewed in great detail and will be presented here only briefly.[35–39] HIV protease mutations that arise in response to treatment conditions must by definition provide a replication advantage. Primary mutations typically include D30N, G48V, I50L/V, V82A/F/T, I84V, and L90M and are commonly found near the active site.[40] They affect hydrophobic, van der Waals, and electrostatic interactions between the enzyme and inhibitor, resulting in a loss of binding affinity that decreases an inhibitor drug's effectiveness.[41,42] However, the mutations also interfere with substrate processing, conferring a fitness cost and negatively affecting the replication of HIV.[43,44] As a result, additional mutations accumulate in a stepwise fashion that restore catalytic efficiency while maintaining drug resistance.[45] Often, these secondary mutations occur further away from the active site causing long-range structural perturbations that compensate for the primary mutation's functional deficit. Additionally, *Gag* and *Gag-Pol* may co-evolve with the protease incurring mutations that enhance their ability to be processed by the mutant protease.[46,47] Ultimately, ten or more mutations can accumulate resulting in viable viruses with resistance to multiple drugs.

2. Targeting the Protein Backbone to Combat Drug Resistance

2.1. The Underlying Principle behind the Backbone-Binding Strategy

We have developed a novel structure-based concept for drug design to address the problem of drug resistance. Our structural analysis and comparison of the X-ray structures of various mutant HIV-1 proteases with the X-ray structure of wild-type HIV-1 protease revealed that the backbone conformation in the active site of mutant proteases is only minimally distorted.[48,49] Conceivably, if we design an inhibitor that maximizes interactions in the HIV protease active site, particularly extensive hydrogen-bonding interactions with the protein backbone of the wild-type HIV-1 protease, such an inhibitor will likely maintain these contacts with mutant proteases. In essence, by targeting the protein backbone, the development of drug-resistant HIV should be hindered, as mutations that alter the backbone conformation would most likely reduce catalytic capacity.[50] We view this designed inhibitor as a "molecular crab" capable of tightly gripping the protein backbone and holding on in the enzyme active site.

This backbone-binding design strategy led to the development of new PIs with enhanced active-site interactions, in particular inhibitor–backbone hydrogen-bonding interactions. Fundamentally, for drug resistance to occur, viral mutations must arise that diminish drug binding but retain viral fitness. Mutations that occur within the active site or result in structural distortions are limited because they produce impaired proteolysis of the natural polyprotein substrates.[43,44] This was reinforced during our reviews of X-ray structures of mutant HIV-1 proteases which revealed the structural changes associated with drug-resistant mutants.[51,52] Based upon this backbone-binding strategy, we have focused our molecular design efforts on promoting extensive hydrogen-bonding interactions with the protein backbone atoms contributing to the S2–S2′ subsites. The S1 and S1′ subsites are largely formed by hydrophobic residues, while both hydrophobic and hydrophilic residues contribute to the S2 and S2′ subsites.[53] In addition, we planned to fill the hydrophobic pockets throughout the protease active site and thus further limit the ability of the virus to develop drug resistance. Furthermore, we have sought to improve bioavailability by decreasing the peptidic character of our inhibitors through the design of heterocyclic or cyclic-polyether-derived templates and ligands. In this Review, we highlight the molecular

basis for this targeted protein-backbone-binding concept and feature our designed inhibitors that have emerged from this novel design concept. Our extensive X-ray crystallographic studies and a detailed analysis of antiviral data strongly corroborate our protein-backbone-binding strategy to combat drug resistance.

2.2. Protein Structure Defines Catalytic Activity

Investigations into the factors controlling enzyme activity have revealed that protein structure and enzyme function are closely related.[54–56] Most enzymes are proteins consisting of strands of amino acids combined to form distinct polypeptide chains. These proteins fold spontaneously, generating local secondary structures (α helix, β strands, etc.) that lead to the formation of a defined three-dimensional (3D) tertiary structure. With many enzymes, multiple protein chains combine through noncovalent interactions forming a quaternary structure possessing multiple subunits. Protein structures are stabilized by a collection of weak intramolecular forces that can be disrupted and reformed allowing a limited range of dynamic movement. The folding process creates cavities near the surface of the enzyme that may serve as substrate binding sites. Interestingly, a relatively small volume of the overall enzyme constitutes the active catalytic site with the remainder of the protein serving as a structural scaffold.[57] For effective catalysis to occur, the amino acid residues within the active site require a specific 3D configuration in which the transition state of the chemical reaction can be attained more readily than in the absence of the enzyme.[58–60] Perturbations of this configuration can have a deleterious effect resulting in a loss of catalytic function. Hence, viral mutations are limited by natural selection requirements to maintain the key structural elements of an enzyme's active site.

2.3. HIV-1 Protease's Substrate Binding Site and Conserved Interactions

HIV-1 protease is an aspartic protease containing two catalytic aspartic acid residues in the active site that share an acidic proton and interact with a water molecule in the absence of a substrate or inhibitor. The catalytically active enzyme is a homo dimer and each monomer comprises 99 amino acids. The active site is formed by two catalytic aspartic acids and each residue is located in each domain (monomer). The scissile bond of the peptide substrate is in close proximity to the active site. A pair of flaps, one from each monomer, is located at the entrance to the active site.[61] The flaps fold down over substrates upon binding and act as a solvent shield that excludes water and creates a local environment conducive to catalysis. The flaps are flexible, showing an open conformation in the apoenzyme.[53,62] The peptide substrate contains at least seven residues extending from P4 to P3′, where the scissile bond lies between P1 and P1′. The side chains of the substrate lie in subsites S4 to S3′ formed by protease residues. Hydrophobic residues occupy the S1 and S1′ subsites, and hydrophobic or hydrophilic residues can be accommodated by the S2 and S2′ subsites. A series of conserved hydrogen-bonding interactions connect the backbone of the protease and the substrate and serve as a major contribution to binding affinity.[63] These interactions are shown in Figure 1. The X-ray structure of HIV protease

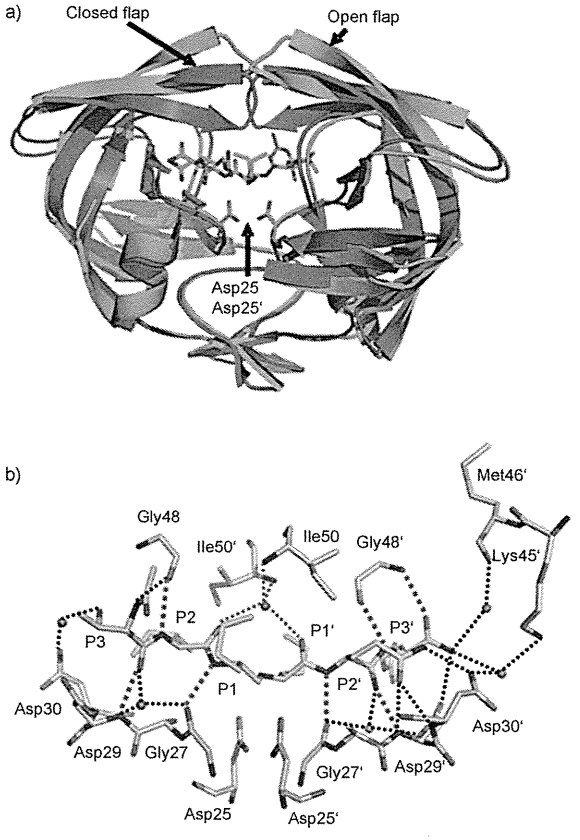

Figure 1. a) Comparison of unliganded protease with open conformation flaps (PDB code 1HHP[64] in cyan) and protease in complex with a substrate analogue (PDB code 2AOD[64] in magenta) showing closed conformation flaps. The catalytic residues Asp25 and Asp25′ and the peptide analogue are shown as stick models. b) Interactions of the protease with the peptide analogue of the p2/NC cleavage site (ace-Thr-Ile-Nle-r-Nle-Gln-Arg, where Nle is norleucine substituting for Met in the natural peptide sequence and r indicates the reduced peptide bond) (PDB code 2AOD).[64] The conserved hydrogen-bonding interactions are shown as green dotted lines, and nonconserved hydrogen bonds are indicated by black dashed lines.

bound to the peptide analogue of the p2/NC cleavage site (PDB code 2AOD) demonstrates these interactions.[64] A number of amino acid residues in the active site, such as Asp25, Gly27, Ala28, Asp29, and Gly48, are highly conserved; therefore, inhibitor design strategies targeting these residues have led to potent PIs.[50,65–68]

2.4. Structural Evidence of Minimal Backbone Distortion in Mutant HIV-1 Proteases

During our efforts in structure-based drug design to develop novel antiviral HIV-1 protease inhibitors, we have

compared the X-ray crystal structures of inhibitor-bound HIV-1 protease (wild type) with the crystal structures of drug-resistant mutants of the protease.[48,49] As stated earlier, superimposition of these structures indicates only a minimal deviation in the backbone atoms around the active site. These structural comparisons provided insight into the molecular design strategy for combating drug resistance as reviewed recently.[50] Mutations can be divided into two main categories. First, mutations of active-site residues can directly alter protease interactions with an inhibitor, as shown by examples of mutants containing I84V or I50V that reduce interactions with a number of PIs.[69–71] Alternatively, distal mutations can act indirectly to diminish protease stability and interactions with an inhibitor, as shown for mutants with L24I, F53L, and L90M.[70,72,73] The majority of these mutants show minimal changes in the backbone structure around the active site. Even the flexible flaps generally show changes of less than 1 Å for the backbone atoms. One exception is mutation V82A, which produces shifts in the loop comprising residues 79–82 with compensating hydrophobic contacts.[71,73,74] The loop can adjust by 1–2 Å to accommodate the different-sized hydrophobic groups at P1 and P1′ of the inhibitors.[75] As depicted in Figure 2, even structures of drug-resistant HIV-1

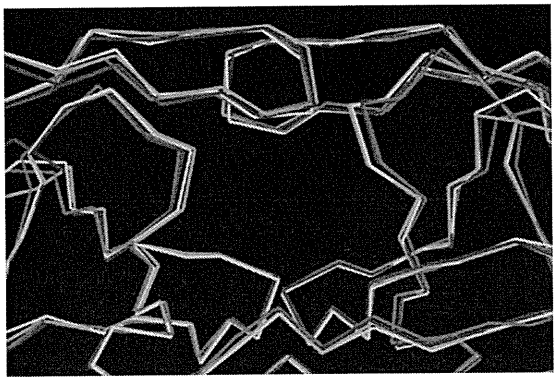

Figure 2. Overlay of HIV-1 protease with multiple mutants (green: PDB code 2FDD;[76,77] yellow: PDB code 1SGU[78]), HIV-2 protease (red: PDB code 1HSH[79]) with HIV-1 protease (blue: PDB code 2IEN[69]) showing minimal backbone deviation.

proteases with 10–14 mutations, and HIV-2 protease which differs in about 40 different residues, superimpose with only a minimal deviation in the backbone atoms around the active site.[51,76–79] Mutations producing drug resistance cannot significantly alter the overall structure of the active site that is essential for protease function. Viable mutant strains will show minimal distortions in the structure of the protease active site as expected in order to maintain catalytic activity and viral replication fitness.[50,52] Based on these observations, we hypothesized that inhibitors that maximize hydrogen-bonding interactions with backbone NH or C=O atoms in the active site would retain these interactions in viral mutants. Therefore, these compounds would maintain potency despite viral mutation, providing a viable solution to the problem of drug resistance in HIV-1 treatments. Using this original design concept, we have actively designed and synthesized a variety of inhibitors that form extensive binding interactions with the protease backbone and are capable of maintaining efficacy against panels of clinically relevant drug-resistant HIV-1 viral strains.[50,67,68,80]

3. Structure-Based Design Targeting the Protein Backbone

3.1. PIs with High-Affinity Ligands Derived from Cyclic Ethers

In an effort to combat drug resistance, we have been involved in the design and synthesis of conceptually novel protease inhibitors based upon the X-ray structure of HIV-1 protease bound to saquinavir (**1**, Figure 3). Our major strategy in structure-based design is to maximize inhibitor

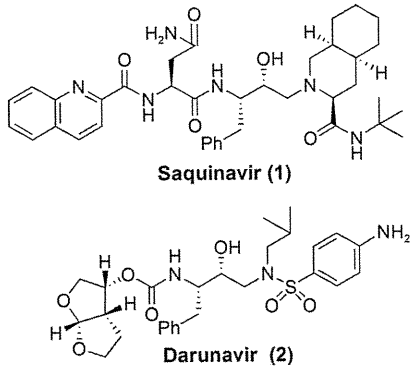

Figure 3. Structures of saquinavir and darunavir.

interactions in the protease active site. Particularly, we planned to promote hydrogen bonding with the protease backbone atoms in the S2 to S2′ subsites.[50] These efforts culminated in the discovery of a wide range of exceedingly potent PIs with impressive resistance profiles. One of these PIs was darunavir (**2**, TMC-114, UIC-94017), which has been approved by the FDA for the treatment of HIV/AIDS patients harboring drug-resistant HIV.[81,82] We have described the development of darunavir in a number of recent reviews.[67,83,84] Here, we will briefly highlight those early structure-based efforts and focus mainly on darunavir's unique binding properties using X-ray crystallographic studies and we will analyze drug-resistance properties in light of the structural information. We will then provide highlights of our subsequent efforts into the design of a variety of PIs using the backbone-binding strategy to develop a new generation of PIs to withstand emerging multidrug-resistant HIV-1 variants.

Initially, our design of PIs focused on reducing the peptide-like features and improving the druglike properties of saquinavir-based protease inhibitors.[67] Saquinavir (**1**) is a potent FDA-approved inhibitor; established structure–activity studies and known X-ray structural information have provided important molecular insight into the ligand-binding interactions.[85,86] On the basis of this structural information, we were particularly interested in reducing the molecular weight and eliminating peptide-like bonds. We drew inspira-

tion from nature and began incorporating cyclic ether features inherent to bioactive natural products.[68] We developed a series of molecular scaffolds featuring conformationally constrained cyclic ether and heterocyclic structures that mimic the binding modes of peptide/amide bonds in the S2 subsite of the HIV-1 protease active site.

3.2. Development of 3S-THF and Bis-THF P2 Ligands

Although saquinavir is a potent PI, its oral bioavailability is poor, possibly because of the presence of multiple amide/peptide bonds. Based upon the X-ray structure of saquinavir-bound HIV-1 protease, we attempted to replace two amide carbonyls (P2/P3) with cyclic ether and sulfone templates. Particularly, we planned to position the ether or sulfone such that the oxygen atom could form interactions with the protease similar to those seen for the P2 and P3 amide/peptide carbonyl functions of saquinavir. We were interested in cyclic ether features because numerous bioactive natural products contain such structural subunits, and natural products such as monensin and ginkolide do not suffer from the absorption problems inherent to peptidelike drugs.[87,88] As shown in Figure 4, replacement of the P2-asparagine of saquinavir with 3*R*-tetrahydrofuranyl glycine resulted in the very potent PI **3** (enzyme $IC_{50} = 0.05$ nM; antiviral $CIC_{95} = 8$ nM). The *R* configuration appeared to be critical to its potency.[89] We then removed the P3-quinaldic ligand and designed the corresponding stereochemically defined urethane derivative **4** ($IC_{50} = 160$ nM; concentration for 95% inhibition in cell culture (CIC_{95}) = 800 nM).[90] This lead structure was quite important as the molecular weight of **4** (515 Da) was much less than that of saquinavir (670 Da).

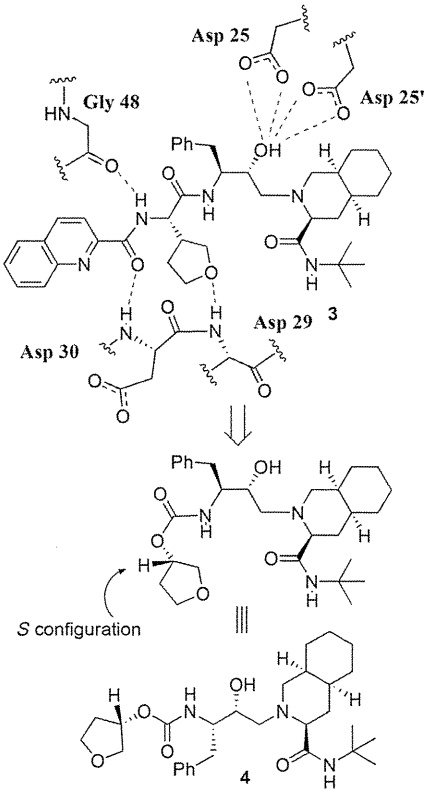

Figure 4. Inhibitors containing a cyclic ether as a P2 ligand.

The 3*S*-THF urethane **4** was significantly more potent (more than 18-fold) than the corresponding *N*-Boc derivative. Incorporation of this functionality in the hydroxyethylene-derived inhibitor **5** resulted in a marked enhancement of enzyme inhibitory and antiviral activity over that of the corresponding *N*-Boc derivative.[90] The cyclopentyl derivative **6** (Figure 5) was significantly less active even though this

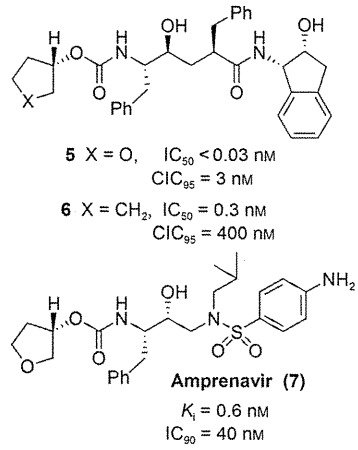

Figure 5. Potent PIs based on 3*S*-THF-urethane.

PI presumably fills the substrate binding site in the same fashion as inhibitor **5**. This result indicated that the cyclic ether oxygen is very important. A preliminary X-ray structure of **4**-bound HIV-1 protease showed that the THF-ring oxygen is involved in a weak hydrogen-bonding interaction with the NH groups of Asp29 and Asp30.[90] Introduction of this 3*S*-THF urethane in the hydroxyethylamine sulfonamide isostere developed by Vasquez et al.[91] and Tung et al.[92] resulted in PI **7** (Figure 5, VX-478).[93] This was subsequently developed into the FDA-approved inhibitor amprenavir/fosamprenavir. The X-ray structure of **7**-bound HIV-1 protease indicated that the ring fills the S2 subsite and the ring oxygen is involved in a weak interaction with the Asp29 and Asp30 backbone amides (distances of 3.4 and 3.5 Å, respectively).[93]

Based upon our preliminary development of 3*S*-THF urethane as a possible substitute for both the P2 and the P3 ligands of saquinavir, we became interested in further enhancing the binding-site interactions in the S2 subsite. This objective ultimately led us to design the stereochemically defined bicyclic (3*R*,3a*S*,6a*R*) tetrahydrofuran (bis-THF) ligand shown in Figure 6.[94] Inhibitor **8** with the (3*R*,3a*S*,6a*R*) bis-THF ligand was significantly more potent than inhibitor **9** containing the (3*S*,3a*R*,6a*S*) bis-THF ligand. Inhibitor **8** was also considerably more potent than inhibitor **4** with 3*S*-THF as the P2 ligand. Our X-ray crystallographic studies revealed that the bis-THF oxygens form effective hydrogen bonds with the backbone NH groups of Asp29 and Asp30.[94] Furthermore, the X-ray structure showed that the bicyclic ring in **8** fills the hydrophobic pocket in the S2 site more effectively than the monocycle in inhibitor **4**. Interest-

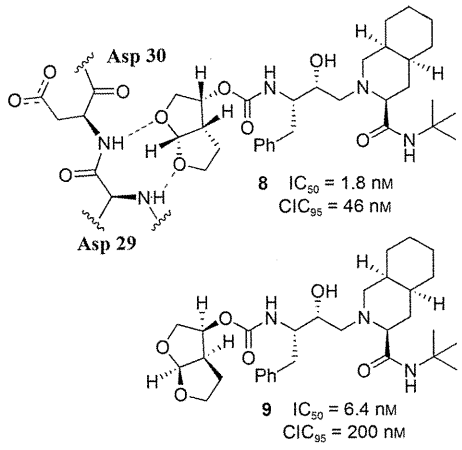

Figure 6. Design of PIs containing a bis-THF ligand.

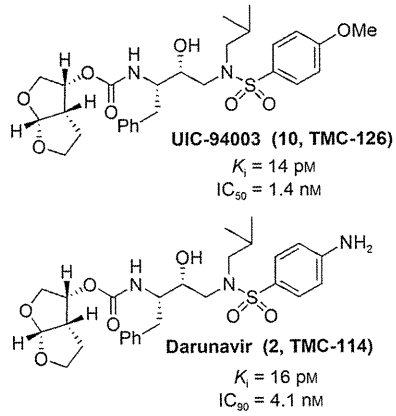

Figure 7. Potent bis-THF PIs, TMC-126 and darunavir.

ingly, however, inhibitor **8** does not form any hydrogen bonds with the protein backbone in the S2′ site.[86,94] As stated earlier, to combat drug resistance, the main emphasis of our backbone-binding strategy is to maximize ligand binding site interactions, especially to promote hydrogen-bond formation with the backbone atoms from the S2 to S2′ subsites of the protease.[50]

3.3. Design of TMC-126 and Its Relevance to the Backbone-Binding Concept

Following the design of the high-affinity and nonpeptidic bis-THF ligand, our next objective was to design an inhibitor that could form robust hydrogen bonds throughout the S2 to S2′ subsites.[50] We investigated the effect of a P2 bis-THF ligand with a number of different isosteres, including (*R*)-(hydroxyethyl)sulfonamide isosteres[91,92] with a *p*-methoxysulfonamide as the P2′ ligand.[50,81] Our initial choice of *p*-methoxysulfonamide was based upon the presumption that the methoxy oxygen would form effective hydrogen bonds with the Asp29′ and Asp30′ backbone NH groups in the S2′ subsite. As shown in Figure 7, inhibitor **10** (UIC-PI or UIC94003 and later TMC-126) exhibited marked enzyme inhibitory potency (K_i = 14 pM) and antiviral activity (ID_{50} = 1.4 nM) in CEM cell lines.[82] To obtain molecular insight into the ligand binding site interactions, a high-resolution X-ray structure of **10**-bound HIV-1 protease was determined.[95] As shown in Figure 8, both oxygen atoms of the P2 bis-THF ligand form strong hydrogen bonds with the backbone NH groups of Asp29 and Asp30 in the S2 subsite. In the S2′ subsite, the *p*-methoxy oxygen also forms strong hydrogen bonds with the backbone NH group of Asp30′ as well as with carboxylate of the the Asp30′ side chain.[95] The inhibitory potency of **10** against numerous mutant HIV proteases was determined. As shown in Table 1, this inhibitor maintained very impressive potency (K_i < 100 pM) and the K_{imut}/K_{iwt} ratios were no greater than 5. This indicated that proteases with multiple mutations, which were shown to be highly resistant to approved first-generation PIs, displayed a low level of resistance against **10**.[96]

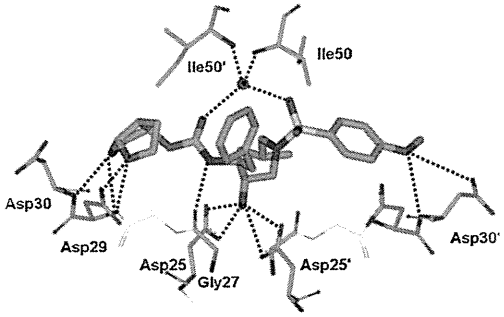

Figure 8. X-ray crystal structure of **10**-bound HIV-1 protease.

Table 1: Enzyme inhibitory potency of **10** against wild-type and mutant proteases.

Enzyme	K_i [pM]	K_{imut}/K_{iwt}	Vitality
wild type	14	1	1
D30N	< 5	0.33	0.3
V32I	8	0.57	0.5
I84V	40	2.85	1
V32I/I84V	70	5	0.7
M46F/V82A	< 5	0.33	0.1
G48V/L90M	< 5	0.33	0.1
V82F/I84V	7	0.5	0.1
V82T/I84V	22	1.57	0.1
V32I/K45I/F53L/A71V/I84V/L89M	31	2.2	0.1
V32I/L33F/K45I/F53L/A71V/I84V	46	3.3	0.1
20R/36I/54V/71V/82T	31	2.2	0.1

Inhibitor **10** also maintained excellent potency against a wide spectrum of drug-resistant HIV-1 variants with IC_{50} values ranging from 0.3 to 0.5 nM.[82] As shown in Table 2, a detailed drug-sensitivity evaluation with **10** demonstrated significant advantages compared to structurally related amprenavir and other approved PIs in terms of the emergence of drug resistance. Interestingly, viral acquisition of resistance to **10** was substantially delayed. Furthermore, **10**-resistant HIV remained sensitive to all approved PIs except amprenavir. Notably, inhibitor **10** retained impressive potency (IC_{50} = 0.5 to 5.5 nM) against multi-PI-resistant HIV-1 strains isolated from patients who were harboring drug-resistant HIV-1.[82]

Table 2: Sensitivities of **10** (TMC-126) against HIV-1 isolated from individuals having previous extensive PI treatment.

Virus[a]	IC_{50} [μM] (fold change)					
	RTV	IDV	SQV	NFV	APV	**10** (TMC-126)
wild type	0.044 (1)	0.013 (1)	0.010 (1)	0.023 (1)	0.025 (1)	0.0007 (1)
1	>1 (>23)	>1 (>77)	0.27 (27)	>1 (>43)	0.27 (11)	0.004 (6)
2	>1 (>23)	0.49 (38)	0.037 (4)	0.33 (14)	0.28 (11)	0.0013 (2)
3	>1 (>23)	0.49 (38)	0.036 (4)	>1 (>43)	0.26 (10)	0.001 (1)
4	>1 (>23)	0.21 (16)	0.033 (3)	0.09 (4)	0.31 (12)	0.0016 (2)
5	>1 (>23)	>1 (>77)	0.31 (31)	0.41 (18)	0.67 (27)	0.0024 (3)
6	>1 (>23)	0.30 (23)	0.19 (19)	>1 (>43)	0.16 (6)	0.0005 (1)
7	>1 (>23)	>1 (>77)	0.12 (12)	>1 (>43)	0.49 (20)	0.0055 (8)
8	>1 (>23)	0.55 (42)	0.042 (4)	>1 (>43)	0.15 (6)	0.001 (1)

[a] Amino acid substitutions identified in the protease-encoding regions of viruses compared to the consensus sequence cited from the Los Alamos database. See reference [82] for details.

We speculated that the impressive activity of **10** against a wide spectrum of drug-resistant HIV variants is because of its robust binding properties in the active site, particularly its extensive interactions with the backbone NH groups of aspartates in the S2 to S2′ subsites.[50] Thus, the backbone-binding strategy promoting extensive hydrogen bonds throughout the active site (S2 to S2′ subsites) may be an intriguing conceptual framework for the design of a new generation of PIs to combat drug resistance.

4. Backbone-Binding Strategy Leading to the Clinical Development of Darunavir to Combat Drug Resistance

4.1. Structural Optimization Leading to Darunavir

Based upon the results of inhibitor **10** (TMC-126), we then explored the combination of the bis-THF ligand and (*R*)-(hydroxyethyl)sulfonamide isosteres with a variety of P2′ sulfonamide functionalities. These ligands were chosen to interact with the backbone atoms in the S2′ site. These efforts led to the design and synthesis of a number of exceptionally potent PIs. However, only inhibitor **2** (Figure 7, later named TMC-114 and then darunavir) exhibited improved pharmacological properties and drug-resistance profiles.[81,97–99] We attributed the unique binding profile of **10** (UIC-94003 or TMC-126) and **2** (UIC-94017 or TMC-114) as the main contributing factor for the antiviral profile which led us to establish the design concept of protein-backbone binding as a promising strategy to overcome drug resistance.[50,100] The following section takes a closer look at the binding of darunavir and its unique antiviral profile.

4.2. Darunavir's Extensive Interactions with the Protease Backbone

Darunavir's enhanced binding affinity ($K_i = 16$ pM) is likely related to its ability to form an extensive network of hydrogen-bonding interactions within the HIV-1 protease active site. A high-resolution X-ray crystal structure of darunavir-bound HIV-1 protease revealed a number of key interactions between darunavir and the protease's backbone atoms.[69] As shown in Figure 9, the bis-THF P2 ligand forms strong hydrogen bonds with the backbone amide NH groups of Asp29 and Asp30, which anchor darunavir to the S2 subsite. On the opposite end, darunavir's *p*-aminosulfonamide interacts with the amide of Asp30′ and the carboxylic acid side chain of Asp30′ thereby stabilizing darunavir within

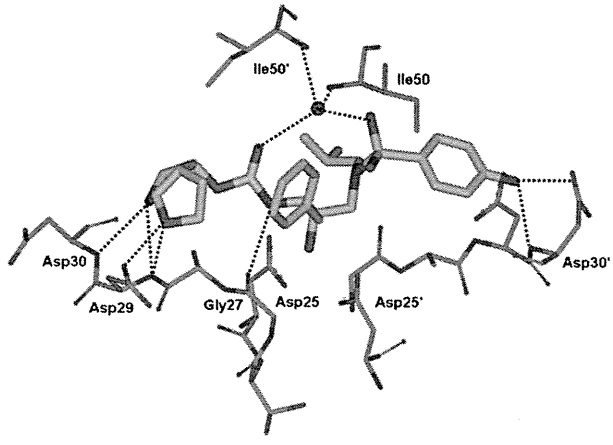

Figure 9. Darunavir binding to HIV-1 protease like a "molecular crab" (PDB code 2IEN).[69]

the active site. The hydroxy group of the (hydroxyethyl)sulfonamide isostere serves as a transition-state mimic forming hydrogen bonds to the catalytic residues Asp25 and Asp25′. In addition, the urethane NH group interacts with the Gly27 carbonyl, while a tetracoordinated water molecule forms hydrogen bonds between flap residues Ile50 and Ile50′ and the urethane carbonyl and sulfonamide oxygen of darunavir. The P1′ isobutyl and P1 benzyl groups of darunavir further enhance binding through hydrophobic interactions.[69] These multiple binding interactions allow darunavir to act as a "molecular crab" tightly clutching the protein backbone.

Unlike many first-generation PIs, the binding of darunavir to HIV-1 protease is unique. For example, while the binding of many PIs is driven by entropic gain, the binding of darunavir is highly enthalpically favored, possibly because of its numerous hydrogen-bonding interactions.[101] Another noticeable difference lies in the kinetics of darunavir's binding to the protease which shows a high association rate and very

slow dissociation rate, much lower than that of other PIs.[102] Together, these attributes provide darunavir with a specific, high-affinity binding profile and an exceptional ability to accommodate protease mutations.[103]

A final distinguishing characteristic of darunavir is that it is capable of binding to the protease at a second location, as indicated by a recent X-ray analysis.[69] The second binding site lies on the surface of the protease on one of its flexible flaps. Allosteric binding at this location may contribute to darunavir's exceptional antiviral activity by further inhibiting the function of the HIV-1 protease. Further studies examined the kinetics of darunavir binding and suggested a mixed-type competitive–uncompetitive inhibition model in contrast to first-generation PIs which exhibit strictly competitive inhibition.[104] These results were consistent with a second binding site for darunavir and likely contribute to darunavir's heightened antiviral activity profile.

4.3. *Darunavir's Robust Potency against Multidrug-Resistant HIV-1 Variants*

Darunavir has demonstrated remarkable antiviral potency across a broad range of HIV-1 viral strains. As depicted in Table 3, against a panel of HIV-1 isolates, darunavir outperformed many other approved PIs at inhibiting viral replication and infectivity (IC_{50} = 3–6 nM).[105] Darunavir's potent antiviral activity combined with its relatively low cytotoxicity provides it with an elevated selectivity index (> 20000 CC_{50}/EC_{50}).[105] More importantly, darunavir has consistently retained its impressive antiviral activity against a host of viral strains with resistance-related mutations. Notably, darunavir exerted very impressive activity against highly multi-PI-resistant clinical HIV-1 variants isolated from patients with AIDS who did not respond to existing antiviral regimens (results are shown in Table 4). Darunavir (**2**) exhibited excellent antiviral activity with IC_{50} values ranging from 3 to 30 nM while APV, IDV, NFV, and RTV, were virtually ineffective in blocking the replication of all multi-PI-resistant strains.[105]

Also, when surveyed against a panel of laboratory HIV-1 strains with selected resistance against other PIs, darunavir maintained excellent activity (Table 5). Only APV-resistant viral strains displayed cross-resistance to darunavir; this can be explained by the fact that APV contains a sulfonamide isostere similar to that in darunavir.[105] More elaborate studies utilizing a broad range of clinical isolates (1500+) further confirmed darunavir's remarkable properties. Darunavir maintained an EC_{50} of less than 10 nM against 75% of the variants and showed less than a tenfold change in EC_{50} compared to the wild-type against 90% of the strains.[106] In contrast, APV, SQV, IDV, RTV, NFV, and LPV displayed ED_{50} values below 10 nM against less than 30% of the viral strains and showed significantly higher levels of variability in the EC_{50} values as compared to the wild-type.[106]

A major challenge in the treatment of HIV remains the rapid emergence of drug resistance which reduces the effectiveness of antiviral treatments. The most prominent attribute of darunavir that sets it apart from other PIs is its high genetic barrier to the development of viral resistance. Early attempts to select for darunavir-resistant HIV viruses in vitro proved difficult; resistance developed very slowly after

Table 3: Sensitivities of **2** and selected anti-HIV agents against HIV-$1_{Ba\text{-}L}$, HIV-2_{ROD}, and HIV-2_{EHO}.

Virus	Cell type	Mean IC_{50} [nM][a] SQV	RTV	IDV	NFV	APV	AZT	DRV (**2**)
HIV-$1_{Ba\text{-}L}$	PBMC	18	39	25	17	26	9	3
HIV-2_{ROD}	MT-2	3	130	14	19	230	18	3
HIV-2_{EHO}	MT-2	6	240	11	29	170	11	6

[a] All assays were conducted in duplicate or triplicate; the data represent mean IC_{50} values from three independent experiments. IC_{50} were evaluated with PHA-PBMC and the inhibition of p24 Gag protein production by the drug as an end point. MT-2 cells were exposed to the virus and cultured, and IC_{50} values were determined by MTT assay. See references [82] and [105] for details.

Table 4: Activity of inhibitor **2** against HIV-1 clinical isolates in PHA-PBMCs.

Virus[a]	IC_{50} values [μM] SQV	APV	IDV	NFV	RTV	DRV (**2**)
HIV-$1_{ERS104pre}$ (wt X4)	0.010	0.023	0.018	0.019	0.027	0.003
HIV-1_{MOKW} (wt R5)	0.004	0.011	0.018	0.033	0.032	0.003
HIV-1_{TM} (MDR X4)	0.23 (23)	0.39	>1 (>56)	0.54 (28)	>1 (>37)	0.004 (1)
HIV-1_{MM} (MDR R5)	0.30 (30)	0.34	>1 (>56)	>1 (>53)	>1 (>37)	0.02 (7)
HIV-1_{JSL} (MDR R5)	0.35 (35)	0.75 (33)	>1 (>56)	>1 (>53)	>1 (>37)	0.029 (10)
HIV-1_{A} (MDR X4)	0.14 (14)	0.16 (7)	>1 (>56)	0.36 (19)	>1 (>37)	0.004 (1)
HIV-1_{B} (MDR X4)	0.31 (31)	0.34 (15)	>1 (>56)	>1 (>53)	>1 (>37)	0.013 (4)
HIV-1_{C} (MDR X4)	0.037 (4)	0.28 (12)	>1 (>56)	0.44 (23)	>1 (>37)	0.003 (1)
HIV-1_{G} (MDR X4)	0.029 (3)	0.25 (11)	0.39 (22)	0.32 (17)	0.44 (16)	0.004 (1)

[a] Amino acid substitutions identified in the protease-encoding regions of viruses compared to the consensus sequence cited from the Los Alamos database. See reference [105] for details.

Table 5: Activity of DRV against PI-resistant HIV-1 laboratory strains.

Virus	Amino acid substitution	EC_{50} [μM][a]					
		SQV	RTV	IDV	NFV	APV	DRV
$HIV\text{-}1_{NL4\text{-}3}$	wild type	0.009	0.018	0.011	0.020	0.027	0.003
$HIV\text{-}1_{SQV5\mu M}$	L10I, G48V, I54V, L90M	>1 (>111)	>1 (>56)	>1 (>91)	0.30 (15)	0.17 (6)	0.005 (2)
$HIV\text{-}1_{RTV5\mu M}$	M46I, V82F, I84V	0.013 (1)	>1 (>56)	0.31 (28)	0.24 (12)	0.61 (23)	0.025 (8)
$HIV\text{-}1_{IDV5\mu M}$	L10F, L24I, M46I, L63P, A71V, G73S, V82T	0.015 (2)	>1 (>56)	>1 (>91)	0.74 (37)	0.33 (12)	0.029 (10)
$HIV\text{-}1_{NFV5\mu M}$	L10F, D30N, K45I, A71V, T74S	0.031 (3)	0.09 (5)	0.28 (25)	>1 (>50)	0.093 (3)	0.003 (1)
$HIV\text{-}1_{APV5\mu M}$	L10F, V32I, M46I, I54M, A71V, I84V	0.020 (2)	>1 (>56)	0.31 (28)	0.21 (11)	>1 (>37)	0.22 (73)

[a] MT-4 cells were exposed to each HIV-1 strain ($100\times TCID_{50}$), and the inhibition of p24 Gag protein production by the drug was used as an end point. Numbers in parentheses represent the fold changes of the IC_{50} values for each isolate relative to that of $HIV\text{-}1_{NL4\text{-}3}$. See reference [105].

multiple passages and only at concentrations of less than 200 nM of darunavir (Figure 10).[106] Later studies showed that although the wild-type HIV virus did not propagate darunavir resistance easily, HIV-1 isolates from antiretroviral-experienced patients were capable of acquiring resistance-related mutations.[107] During the POWER clinical trials, 11 amino acid substitutions were correlated to darunavir resistance including V11I, V32I, L33F, I47V, I50V, I54L/M, G73S, L76V, I84V, and L89V, of which I50V, I54M/L, L76V, and I84V are considered the major mutations.[108,109] A28S was later identified as an amino acid substitution distinctly associated with darunavir and not caused by other PIs.[110] By itself, A28S results in a significant reduction in enzyme fitness which can be restored in part by the secondary mutation I50V. Darunavir resistance to A28S is believed to occur from a shift in position of the P2 sulfonamide that alters its ability to hydrogen bond with the protease causing a decrease in binding affinity.

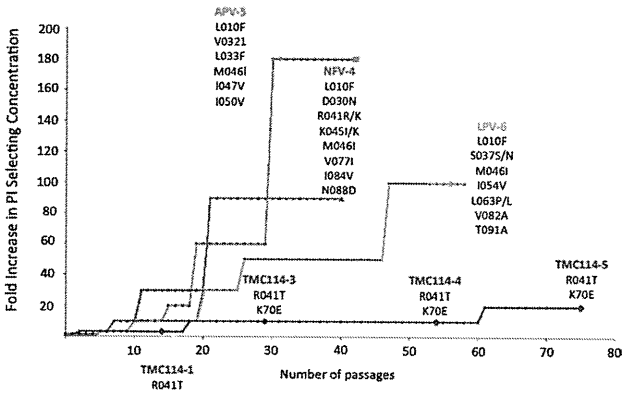

Figure 10. In vitro selection of resistant HIV strains in the presence of NFV, APV, LPV, and TMC-114(DRV). The figure is modified from Figure 4 in reference [106].

4.4. Darunavir Inhibits Dimerization of HIV-1 Protease

Darunavir's impressive antiviral profile can be attributed in part to its small flexible conformation and its ability to form extensive hydrogen-bonding interactions with the protease backbone, which imparts a high binding affinity. Another contributing factor is darunavir's unique ability to act as a dual inhibitor, blocking not only the cleavage of the natural peptide substrate but also inhibiting dimerization of the HIV-1 protease. An active HIV-1 protease consists of two chains of 99 amino acids each that combine or dimerize into a single catalytically active quaternary structure. Dimerization of the monomer subunits is essential for activity and thus its inhibition represents a distinct mechanism for inhibiting viral replication.[111] Darunavir blocks this dimerization process at concentrations as low as 0.01 μM.[112] Further investigation is currently ongoing. TPV is the only other PI besides darunavir that has been shown to possess this property.[112] While capable of blocking the dimerization of individual monomers, neither darunavir nor TPV is able to cause disassociation of an assembled protease unit.

5. Retaining Backbone Binding and Designing Exceptionally Potent Bis-THF-Derived PIs

5.1. The Effect of Benzodioxolane Sulfonamide at the S2′ Site

We continued to explore structural modifications that would form additional hydrogen bonds with the protease backbone residues leading to inhibitors with higher affinity. We have incorporated a benzodioxolane sulfonamide as the P2′ ligand and this has provided inhibitor **11** (GRL-98065) shown in Figure 11. This turned out to be an exceedingly potent inhibitor with significant antiviral activity ($K_i = 11$ pM and $IC_{50} = 1.1$ nM).[113] As can be seen in Table 6, inhibitor **11** was evaluated against a wide spectrum of multidrug-resistant clinical isolates and inhibitor **11** outperformed other approved PIs including darunavir. It maintained significant antiviral activity (6–12-fold change) similar to darunavir. Furthermore, **11** was evaluated against PI-resistant HIV-1 variants and was found to have a unique antiviral activity profile (Table 7). Against the PI-resistant variants, cross-resistance to APV was observed. Interestingly, SQV and ATV remained active against viral strains selected against **11** which contain the A28S mutation. This was linked to TMC-126 resistance and resulted in a significant loss in fitness of the protease.[113]

We determined the crystal structure of **11**-bound HIV-1 protease at 1.6 Å resolution. This structure has provided important molecular insight into the inhibitor potency and

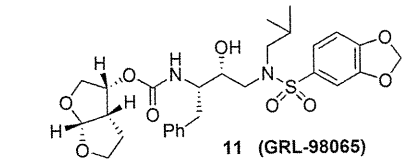

11 (GRL-98065)
K_i = 11 pM
IC_{50} = 1.1 nM

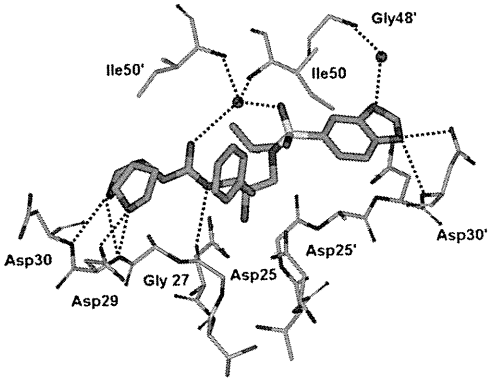

Figure 11. Structure of **11** and the X-ray crystal structure of **11**-bound HIV-1 protease.

drug-resistance profile.[113] Structural analyses revealed that **11** is involved in extensive interactions with the backbone atoms of the amino acids in the protease active site (Asp29 and Asp30, Figure 11) in the S2 to S2′ subsites. These interactions are important for its potency and wide-spectrum activity against multi-PI-resistant HIV-1 variants. Moreover, these interactions are maintained in crystal structures of **11**-bound drug-resistant mutants.[114] Comparison of the crystal structure of **11** with the crystal structure of darunavir (Figure 9) showed that the interactions with the S2 site are similar, but the nature of the hydrogen bonds with residues differs in the S2′ region. A water-mediated interaction of one of the benzodioxolane oxygens with flap residue Gly48′ is not observed for darunavir (**2**). These differences in interactions may account for the improvement of IC_{50} values of **11** compared to those of darunavir.[113]

5.2. Design and Clinical Development of Bis-THF PIs with Novel P1 Functionalities

Numerous potent PIs have been designed based upon the privileged bis-THF ligand.[67,84] As shown in Figure 12, brecanavir (**12**; BCV/GW0385), which was developed by Glaxo Smith Kline, contains a bis-THF P2 ligand, a benzodioxolane P2′ ligand, and a substituted P1 ligand.[115,116] It showed femtomolar enzyme inhibitory potency (K_i = 15 fM) and subnanomolar antiviral activity with an IC_{50} value of 0.7 nM (wild-type virus). Also, BCV exhibited IC_{50} values of 1.1 nM and 4.8 nM against two MDR viral strains, EP13 HIV-1 and D545701 HIV-1, respectively.[115] BCV exhibited sub- to

Table 6: Antiviral activities of GRL-98065 (**11**) against multidrug-resistant clinical isolates.

Virus[a]	EC_{50} [nM][b]					
	SQV	RTV	NFV	APV	DRV	**11** (GRL-98065)
HIV-$1_{ERS104pre}$ (wild-type X4)	8	25	15	29	3.8	0.5
HIV-$1_{MDR/TM}$ (X4)	180 (23)	>1000 (>40)	>1000 (>67)	300 (10)	4.3 (1)	3.2 (6)
HIV-$1_{MDR/MM}$ (R5)	140 (18)	>1000 (>40)	>1000 (>67)	480 (17)	16 (4)	3.8 (8)
HIV-$1_{MDR/JSL}$ (R5)	290 (36)	>1000 (>40)	>1000 (>67)	430 (15)	27 (7)	6 (12)
HIV-$1_{MDR/B}$ (X4)	270 (34)	>1000 (>40)	>1000 (>67)	360 (12)	40 (11)	3.9 (8)
HIV-$1_{MDR/C}$ (X4)	35 (4)	>1000 (>40)	420 (28)	250 (9)	9 (2)	2.7 (5)
HIV-$1_{MDR/G}$ (X4)	33 (4)	>1000 (>40)	370 (25)	320 (11)	7 (2)	3.4 (7)

[a] The amino acid substitutions identified in the protease-encoding region compared to the consensus type B sequence cited from the Los Alamos database. See reference [113] for details. [b] Effective concentration by 50%.

Table 7: Antiviral activities of **11** against laboratory PI-resistant HIV-1 variants.

Virus	EC_{50} [μM] of drug[a]								
	SQV	RTV	IDV	NFV	APV	LPV	ATV	DRV	**11** (GRL-98065)
HIV-1_{NL4-3}	0.007	0.033	0.034	0.033	0.026	0.031	0.0042	0.0030	0.0003
HIV-$1_{SQV5\mu M}$	>1 (>143)	>1 (>30)	>1 (>29)	0.48 (15)	0.33 (13)	0.27 (9)	0.326 (78)	0.0058 (2)	0.006 (20)
HIV-$1_{RTV5\mu M}$	0.010 (1)	>1 (>30)	0.25 (7)	0.21 (6)	0.28 (11)	0.16 (5)	0.018 (4)	0.018 (6)	0.0025 (8)
HIV-$1_{IDV5\mu M}$	0.059 (8)	>1 (>30)	>1 (>29)	0.47 (14)	0.17 (7)	0.26 (8)	0.06 (14)	0.015 (5)	0.0037 (12)
HIV-$1_{NFV5\mu M}$	0.024 (3)	0.051 (2)	0.27 (8)	>1 (>30)	0.060 (2)	0.024 (1)	0.021 (5)	0.0033 (1)	0.0024 (8)
HIV-$1_{APV5\mu M}$	0.031 (4)	0.29 (9)	0.200 (6)	0.27 (8)	>1 (>38)	0.23 (7)	0.003 (1)	0.33 (110)	0.032 (107)
HIV-$1_{LPV1\mu M}$	0.032 (5)	>1 (>30)	>1 (>29)	0.49 (15)	0.31 (12)	0.31 (10)	0.040 (10)	n.d.	0.0075 (25)
HIV-$1_{ATV1\mu M}$	0.037 (5)	0.12 (4)	0.388 (11)	0.22 (7)	0.20 (8)	0.033 (1)	0.33 (79)	0.0034 (1)	0.0015 (5)
HIV-$1_{GRL98065p40}$	0.032 (5)	0.38 (12)	0.28 (8)	0.34 (10)	>1 (>38)	0.19 (6)	0.011 (3)	0.21 (70)	0.18 (600)

[a] MT-4 cells were exposed to 100 $TCID_{50}$ (dose for 50% infection in cell culture) of each HIV-1, and inhibition of p24 Gag protein production by each drug was used as an end point. Numbers in parentheses represent *n*-fold changes in the EC_{50} values for each isolate compared to the EC_{50} values for wild-type HIV-1_{NL4-3}. All assays were conducted in duplicate or triplicate, and data shown are derived from the results of three independent experiments. n.d. = not determined. See reference [113] for details.

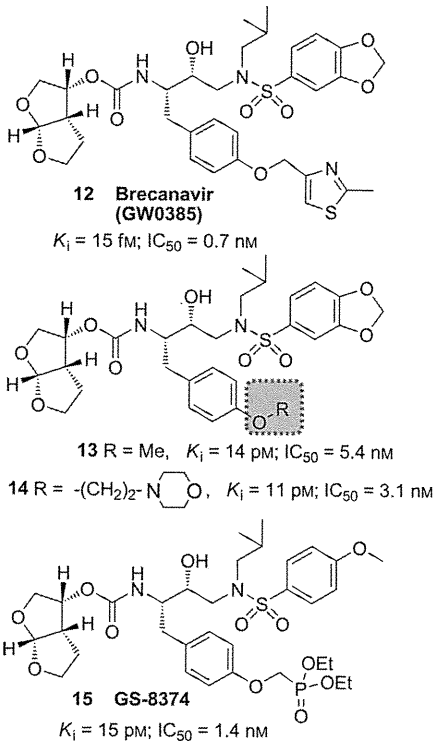

Figure 12. Structures of PIs **12–15.**

low nanomolar IC_{50} values with low cross-resistance against a panel of 10 highly resistant and specifically PI-resistant HIV-1 isolates.[115] Furthermore, BCV was tested against a panel of 55 clinical isolates from PI-experienced patients and it maintained low nanomolar IC_{50} values (0.1–14.9 nM) for all isolates. The majority of isolates (80%) displayed IC_{50} values at or below 0.8 nM.[117,118] This inhibitor had undergone clinical development at the phase III level. However, brecanavir's clinical trials were terminated because of formulation issues.[119]

We have investigated structure-based modifications of the P1 side chain of inhibitor **11**. Of particular interest, we attempted to incorporate a basic amine or a cyclic ether functionality to improve aqueous solubility and other pharmacological properties. Both PIs **13** and **14** have shown very potent antiviral activity.[120]

Inhibitor **15** (GS-8374) containing a P2 bis-THF unit, a P2′ *p*-methoxybenzesulfonamide ligand, and a diethylphosphonylmethoxy group attached to the P1 phenyl ligand was developed by researchers at Gilead Sciences.[121] The phosphonate functionality was designed to promote better intracellular retention without interfering with the protease binding site of **10** (TMC-126). This PI (**15**) displayed an excellent resistance profile.[121,122] It exhibited a mean 6.2-fold change in EC_{50} values (range 0.6–26 nM) from the wild-type HIV. Inhibitor **15** displayed a mean 29.8-fold change (1.0–157 nM) and 23.6-fold change of EC_{50} values (1.2–121 nM) compared to darunavir and BCV, respectively. Towards a possible explanation of this marked resistance suppression, it was proposed that the phosphonate moiety acted as an anchor point in the solvent medium and enhanced the degeneracy of the binding state of the inhibitor by providing favorable entropic compensation following protease mutations. Interestingly, selection of HIV-1 strains exposed to **15** did not exhibit any signs of RAM (resistance-associated mutation) even after six months.[123] GS-8374 has been reported to show more favorable pharmacological and metabolic profiles than other PIs. In the X-ray crystal structure of **15**-bound HIV-1 protease the binding profiles for the P2 bis-THF and the P2′ methoxysulfonamide ligands are similar to those observed in the X-ray structure of the **10**-bound HIV-1 protease. A comparison of the two structures showed that one of the phosphonate ethyl moieties of **15** is bound in a hydrophobic cleft on the surface of protease.[121] GS-8374 with a *p*-diethylphosphonate at the P1 phenyl residue exhibited a better resistance profile than to BCV, which contains a substituted methylthiazole at P1.[123]

5.3. The Effect of a C4-Methoxy Bis-THF Ligand at the S2 Site

The HIV-1 protease flaps are flexible in the apoenzyme form, but they are closed when inhibitors bind and show minimal change in their backbone conformation.[53,124] As can be seen in Figure 11, a novel water-mediated interaction with Gly48' through the benzodioxolane oxygen may be responsible for its superb antiviral and drug-resistance profile. Based upon the X-ray structure of **10**-bound HIV-1 protease, we envisioned that heteroatom-containing substituents at the C4 position of the bis-THF ligand would be ideally positioned to interact with the backbone NH group of Gly48.[95] Therefore, we synthesized a series of new PIs incorporating C4-alkoxy-substituted bis-THF ligands.[125] As shown in Figure 13, inhibitor **16** with a 4*R*-methoxy group has better enzyme inhibitory potency (K_i = 2.9 pM) than inhibitor **10** (K_i = 14 pM). The 4*R* isomer **16** was 12-fold more potent than the corresponding 4*S* isomer **17**. Larger alkyl groups at C4, such as benzyloxy substituents, led to significant reduction in potency. An X-ray structure of **16**-bound HIV-1 protease (Figure 13) showed extensive interactions of the inhibitor with the protease active site similar to those of inhibitor **10**.[125] However, it appears that the oxygen of the 4*R*-methoxy group forms a unique water-mediated hydrogen bond with the NH group of Gly48. The improvement in binding affinity of **16** may be due to this water-mediated hydrogen bond with the backbone NH group of Gly48.[125]

5.4. Design of Macrocyclic Inhibitors with a Bis-THF Unit at the S2 Site

In an effort to fill the hydrophobic pocket in the S1′–S2′ subsites with flexible macrocycles, we investigated bis-THF-derived macrocyclic inhibitors involving P1′–P2′ ligands that can retain all major hydrogen-bonding interactions with the protein backbone similar to those of inhibitor **10** and darunavir but effectively fill the hydrophobic pocket in the S1′ and S2′ subsites.[95] The design perception for these macrocycles evolved from the observation that certain mutations lead to decreased van der Waals interactions and an increase in size of the hydrophobic pocket in the S1′